This document is the unedited Author's version of a Submitted Work that was subsequently accepted for publication, Applied Surface Science copyright © Elsevier Online after peer review. To access the finaledited and published work see https://www.sciencedirect.com/science/article/pii/S0169433216306675?via%3Dihub
https://doi.org/10.1016/j.apsusc.2016.03.176

Surface sensitivity of elastic peak electron spectroscopy

A. Jablonski*

Institute of Physical Chemistry, Polish Academy of Sciences, ul. Kasprzaka 44/52,

01-224 Warsaw, Poland

(e-mail: ajablonski@ichf.edu.pl)

Abstract

New theoretical model describing the sampling depth of elastic peak electron spectroscopy (EPES) has been proposed. Surface sensitivity of this technique can be generally identified with the maximum depth reached by trajectories of elastically backscattered electrons. A parameter called the penetration depth distribution function (PDDF) has been proposed for this description. Two further parameters are descendant from this definition: the mean penetration depth (MPD) and the information depth (ID). From the proposed theory, relatively simple analytical expressions describing the above parameters can be derived. Although the Monte Carlo simulations can be effectively used to estimate the sampling depth of EPES, this approach may require a considerable amount of computations. In contrast, the analytical model proposed here (AN) is very fast and provides the parameters PDDF, MPD and ID that very well compare with results of MC simulations. As follows from detailed comparisons performed for four elements (Al, Ni, Pd and Au), the AN model practically reproduced complicated emission angle dependences of the MPDs and the IDs, correctly indicating numerous maximum and minimum positions. In the energy range from 200 eV to 5 keV, the averaged percentage differences between MPDs obtained from the MC and the AN models were close to 4%. An important conclusion resulting from the present studies refers to

http://rcin.org.pl

the procedure of determination of the inelastic mean free path (IMFP) from EPES. Frequently, the analyzed sample is deposited as a thin overlayer on a smooth substrate. From an analysis of the presently obtained IDs, is follows that 99% of trajectories in analyzed experimental configurations reaches depth not exceeding 2.39 in units of IMFP. Thus, one can postulate that a safe minimum thickness of an overlayer should be larger than about 3 IMFPs. For example, the minimum thickness of an Al overlayer shoud be about 8 nm at 5000 eV.

Keywords: Theory of electron transport in solids; Monte Carlo simulations; penetration depth of backscattered electrons; inelastic mean free path.

Introduction

The surface sensitive electron spectroscopies, X-ray photoelectron spectroscopy (XPS) and Auger electron spectroscopy (AES) are very useful tools for studies of nanostructures due to small sampling depths of both techniques. Analysis by XPS and AES is extended over only several atomic layers of the surface region. To quantify the thickness of the analyzed layer, we need to know a parameter that characterizes the "survival" of signal electrons in condensed matter. The relevant parameter used for that purpose, the inelastic mean free path (IMFP), is defined as "... average distance that an electron with a given energy travels between successive inelastic collisions" [1]. A voluminous material on the theoretical and experimental IMFP values is presently available. It has been postulated [2] that the IMFPs that are in agreement with the ISO definition can actually be obtained from two methods: (i) the IMFPs calculated from experimental optical data, and (ii) the IMFPs measured by elastic peak electron spectroscopy (EPES). A very extensive set of calculated IMFPs has been published by Tanuma and coworkers for elements [3-5], inorganic compounds [6], and organic compounds [7]. The calculated IMFPs obtained from different theoretical models are also compiled in the NIST database [8]. One should stress here that these IMFPs refer to the

http://rcin.org.pl

bulk of a solid. The IMFPs of electrons in the surface region may be different than in the bulk due to differences in the mechanism of energy losses. Consequently, the signal intensity of surface sensitive electron spectroscopies, X-ray photoelectron spectroscopy and Auger electron spectroscopy, may be affected by the surface energy losses. Quantification of XPS and AES require knowledge of the IMFPs for signal electrons. One can use the calculated IMFPs for that purpose, however it is postulated that they should be additionally corrected for surface energy losses [9-14]. Relatively simple analytical expressions were proposed for the relevant correction: the surface excitation parameter (SEP) [10-13], yet the coefficients needed for these expressions were determined for a limited number of solids. Werner et al. [12] made an attempt to derive a predictive formula for SEP, however its accuracy is generally unknown; it can only be considered as a useful guidance.

In contrast to the calculated IMFPs, the IMFPs obtained from EPES measurements refer to a thin surface region. We expect that the thickness of the layer sampled by backscattered electrons should be comparable to the surface sensitivity of XPS and AES, or even smaller since the elastically backscattered electrons pass the surface layer twice, and thus the probability of an energy loss is larger than that of photoelectrons and Auger electrons. An obvious question arises as to what is the actual sampling depth of EPES measurements. This problem has been approached by Jablonski and Powell [15]. It has been proposed that a convenient measure of the sampling depth of EPES is the penetration depth distribution function (PDDF) [15]. This function was defined as "... the probability that an electron incident on the surface at an angle Θ_0 will be elastically backscattered from a maximum depth z and emitted in the direction of the analyzer at an angle α and not be inelastically scattered". The PDDF, $\xi(z,\alpha,\Theta_0)$, can be normalized so that the integral over depth is equal to the elastic backscattering probability, $\eta(\Delta\Omega)$, measured within a certain solid acceptance angle of an analyzer, $\Delta\Omega$:

$$\int_0^\infty \xi(z,\alpha,\theta_0)\, dz = \eta(\Delta\Omega)\,. \tag{1}$$

http://rcin.org.pl

Two useful parameters were proposed to quantify the sampling depth of EPES, both related to the PDDF [15]. The mean penetration depth (MPD) was defined as a mean value of the PDDF:

$$G = \frac{\int_0^\infty z\xi(z,\alpha,\Theta_0)\, dz}{\int_0^\infty \xi(z,\alpha,\Theta_0)\, dz} \tag{2}$$

Note that this parameter has a close similarity to the parameter called the mean escape depth (Ref. [1], definition 4.203) which characterizes the sampling depth of AES and XPS. The emission depth distribution function in this definition is simply replaced by the PDDF. Second parameter that describes the sampling depth of EPES is the information depth (ID). This parameter, again by analogy with XPS and AES, is defined as a thickness penetrated by a specified percentage, p_{ID}, (for example, equal to 90%, 95% or 99%) of electron trajectories in particular measurement conditions. The ID can be determined by solving the following equation:

$$\frac{\int_0^T \xi(z,\alpha,\Theta_0)\, dz}{\int_0^\infty \xi(z,\alpha,\Theta_0)\, dz} = \frac{p_{ID}}{100} \tag{3}$$

In experiments involving elastic electron backscattering, we often use samples prepared as overlayers deposited galvanically [13] or by vacuum evaporation [13,16] to ensure high smoothness of the studied surface. However, we have to make sure that an overlayer is of sufficient thickness at a given electron energy to avoid influence of the substrate on results of EPES experiments. It has been demonstrated that the sampling depth of EPES may be dramatically affected by the substrate in certain experimental configurations when the overlayer thickness is too small [17]. A safe thickness of an overlayer can be determined experimentally by measuring the elastic backscattering intensity in a given experimental geometry and for an electron energy of interest [18,19], however such

http://rcin.org.pl

experiments are very elaborate and thus are not useful as a guidance in practical EPES analysis.

An electron transport in the surface region of solids can be well characterized by Monte Carlo simulations. This computational tool is proved to accurately predict characteristics of elastically backscattered electrons (angular distribution [16,18,20], energy dependence [21,22] and overlayer thickness dependence of signal electrons [18,19]). In fact, the Monte Carlo algorithms with different simulation strategies are almost exclusively used in calculations of the IMFPs from EPES measurements [2,20,23-25]. It has been shown that, on minor modification, these algorithms can be used for estimation of the EPES sampling depth [15]. However, the Monte Carlo simulations generally require a considerable amount of computations, especially in cases when the EPES measurements are performed with analyzers having small solid acceptance angle. Consequently, such approach is impractical as a routine criterion for estimating a needed thickness of a sample material under study. On the other hand, a simple analytical model, in which only one elastic scattering event is considered, leads to the estimates of the EPES sampling depth that may dramatically deviate from predictions of the Monte Carlo approach. In the present work, an attempt is made to derive an analytical formalism that has accuracy similar to Monte Carlo simulations, however it is relatively simple to use. Furthermore, the relevant calculations are expected to be much faster than the performance of the Monte Carlo algorithms.

2. Theory

Let us consider here the theoretical models that can be used for description of the sampling depth of EPES measurements. At first, let us briefly outline the theoretical models that were used in published calculations of the MPD and EPES ID [15].

2.1. The single large-angle backscattering model

http://rcin.org.pl

We start with the simplest model for the elastic backscattering event designated further here with the acronym SLAB. The formalism is based on two assumptions:

1. Along the trajectory of an elastically backscattered electron, only one large-angle scattering event occurs.

2. Probability of an elastic scattering event along trajectory is much smaller than the probability of inelastic interaction.

The shape of the corresponding trajectory is shown in Fig. 1. The elastically backscattered current within a small analyzer acceptance angle is then given by [15,26]

$$\eta(\Delta\Omega) = \Delta\Omega \frac{\cos\alpha}{\cos\Theta_0 + \cos\alpha} \; N \, \lambda_{in} \frac{d\sigma_{el}}{d\Omega} \tag{4}$$

where N is the atomic density, λ_{in} is the IMFP, and $d\sigma_{el}/d\Omega$ is the differential elastic scattering cross section (DCS). The PDDF is readily obtained from Eqs (1) and (4)

$$\xi(z,\alpha,\Theta_0) = \frac{\Delta\Omega \; N}{\cos\Theta_0} \frac{d\sigma_{el}}{d\Omega} \; \exp\left[-\frac{z}{\lambda_{in}} \left(\frac{1}{\cos\Theta_0} + \frac{1}{\cos\alpha} \right) \right] \tag{5}$$

The MPD and the ID derived from Eqs (2), (3) and (5) have the following form [15]

$$G = \lambda_{in} \frac{\cos\Theta_0 \, \cos\alpha}{\cos\Theta_0 + \cos\alpha} \tag{6}$$

$$T = -\lambda_{in} \frac{\cos\Theta_0 \, \cos\alpha}{\cos\Theta_0 + \cos\alpha} \; \ln\left(1 - \frac{p_{ID}}{100} \right). \tag{7}$$

We note that the MPD and the ID are fully determined by the IMFP and the measurement geometry. The elastic scattering effects are not included this formalism.

2.2. The Monte Carlo model

Theoretical models implemented in Monte Carlo (MC) algorithms are considered to be the most realistic, and consequently, the results obtained from simulations are expected to be the most accurate. Details of such calculations were frequently reported [2,15,20-22,25-27]. The implemented strategies of simulations may differ in different algorithms, however the common assumptions are the following (see Fig. 2):

http://rcin.org.pl

1. An electron changes direction due elastic interaction with a scattering centre of a solid. The probability density function of the polar scattering angles, θ, is expressed by the differential elastic cross section for isolated atoms

$$H(\theta) = \frac{1}{\sigma_{el}} \frac{d\sigma_{el}}{d\Omega} = 2\pi \frac{1}{\sigma_{el}} \frac{d\sigma_{el}}{d\Omega} \sin\theta \tag{8}$$

where σ_{el} is the total elastic cross section

$$\sigma_{el} = \int_{4\pi} \frac{d\sigma_{el}}{d\Omega} d\Omega \tag{9}$$

2. The azimuthal scattering angles, φ, are described by the uniform distribution.

3. An electron trajectory follows the Poisson stochastic process; consequently the linear distances between elastic scattering events, are distributed exponentially

$$F(\Lambda) = \frac{1}{\lambda_{el}} \exp\left(-\frac{\Lambda}{\lambda_{el}} \right) \tag{10}$$

where λ_{el} is an electron elastic mean free path

$$\lambda_{el} = (N\sigma_{el})^{-1} \tag{11}$$

As follows from Fig. 2, to simulate an electron trajectory, one should design samplers of three random variables, i.e. $\sphericalangle$, φ and θ.

To estimate the PDDF, the following weights should be ascribed to each trajectory

$$\Delta\xi_k(z) = \begin{cases} \exp(-x_k / \lambda_{in}) & \text{if an electron entered the analyzer after reaching the maximum depth } z \\ 0 & \text{in all other cases,} \end{cases} \tag{12}$$

where x_k is the length of the kth trajectory. The PDDF is finally calculated from:

$$\xi(z, \alpha, \Theta_0) = \frac{1}{n} \sum_{k=1}^{n} \Delta\xi_k(z) \tag{13}$$

where n is the total number of trajectories. The PDDF resulting from the Monte Carlo simulations can be then used in calculations of the MPD and the ID from Eqs (2) and (3), respectively.

http://rcin.org.pl

2.3. Advanced analytical model

The elastic backscattering probabilities, $\eta(\Delta\Omega)$, have typically small values and obviously depend on the size of an analyzer acceptance solid angle. For example, the ratio $\eta(\Delta\Omega)/\Delta\Omega$ calculated from the MC method for Au at 2000 eV assuming normal incidence of the primary beam and the emission angle, $\alpha = 45°$, is equal to 6.15×10^{-3} (Fig. 7 of ref. [26]). For an analyzer with conical acceptance angle having the half-cone angle equal to 5°, the elastic backscattering probability is equal then to 1.471×10^{-4}. The SLAB theory predicts the value of 2.052×10^{-5} for the same solid angle, which is smaller by a factor of about 7. In effect, the Monte Carlo simulations require considerable amount of computations since the estimated probabilities are very low, especially in the case of small solid angles. This problem becomes more acute in the case of calculations of the PDDF since the number of electrons entering the analyzer solid angle is further distributed with respect to the maximum depth reached. A considerable number of trajectories must be generated to obtain the PDDF with a reasonable precision. A technical problem arises then with the design of the samplers of needed random variables. These samplers must be based on a random number generator with a very extended period. An attempt is made here to propose an analytical theoretical model with accuracy comparable to Monte Carlo algorithm, however with much faster performance.

Let us consider an experimental configuration with normal incidence of the primary beam. Such geometry was frequently used in for determination of the IMFP from EPES measurements [2,20,24,25]. We simplify the assumptions implemented in Monte Carlo simulation strategies:

1. The trajectory of an electron leaving the solid is described by a Poisson stochastic process, however only one large-angle scattering event changes the electron direction. Remaining elastic collisions do not influence the trajectory shape.

2. If k elastic collisions occurred along trajectory of an electron leaving the solid, the angular distribution of electron directions with respect to the direction of the primary beam is derived

http://rcin.org.pl

taking into account all actual probability density functions describing consecutive single elastic scattering events.

An example of an electron trajectory illustrating the above assumptions is shown in Fig. 3.

It has been shown that the above assumptions lead to analytical expressions describing the elastic backscattering probability [20,26,28]. Furthermore, the elastic backscattering probabilities calculated from an analytical model based on similar assumptions very well compare with the measured elastic backscattering probabilities for typical experimental geometries and probabilities obtained from Monte Carlo simulations [20,26]. The ratios of the elastic backscattering probabilities calculated from an analytical model and from Monte Carlo simulations for different pairs of elements were found to differ on average by 3.1% [26]. The mean percentage difference between the measured elastic backscattering probabilities and probabilities obtained from an analytical formalism, averaged over different elements and energies, was equal to 8.8% [26]. We may expect that the parameters describing the surface sensitivity of EPES derived from the above model would also be described with a reasonable accuracy. An advantage of such approach would be a considerable decrease of the needed computing times.

Suppose that an electron elastically backscattered from a solid suffered k elastic scattering events, and suppose that the large angle collision that is expected to occur along the trajectory length took place at a depth z. Let us assume that this is the i-th collision counted along the trajectory after an electron entered the solid. Thus, the distance equal to z is in fact the sum of i linear distances, each with the length, Δz, distributed exponentially (see Fig. 3)

$$g(\Delta z) = \frac{1}{\lambda_{el}} \exp\left(-\frac{\Delta z}{\lambda_{el}} \right) \tag{14}$$

where λ_{el} is the elastic mean free path. Probability density function of the distance equal to the sum of i distances Δz is given by the Erlang distribution [29]

$$f(\Delta z) = \frac{1}{\lambda_{el}} \frac{(z/\lambda_{el})^{i-1}}{(i-1)!} \exp\left(-\frac{\Delta z}{\lambda_{el}} \right) \tag{15}$$

http://rcin.org.pl

Let us denote by y the linear path of an electron towards the surface. Probability that $k-i$ elastic collisions occur along the distance y is given by the Poisson distribution

$$W_{k-i}(y) = \frac{(y/\lambda_{el})^{k-i}}{(k-i)!} \exp\left(-\frac{y}{\lambda_{el}}\right) \tag{16}$$

For the emission angle of backscattered electron equal to α, we have $y = z/\cos\alpha$ and Eq. (16) can be rewritten as follows

$$W_{k-i}(y) = \frac{1}{(\lambda_{el})^{k-i}} \frac{1}{\mu^{k-i}(k-i)!} z^{k-i} \exp\left(-\frac{z}{\mu\lambda_{el}}\right) \tag{17}$$

where $\mu = \cos\alpha$. The probability that an electron leaving the solid was submitted to k elastic scattering events among which i-th interaction was the large angle collision at a depth z is expressed by

$$p_k^i(z) = f_i(z) W_{k-i}(y) = \frac{1}{(\lambda_{el})^{k-i}} \frac{1}{\mu^{k-i}(i-1)!(k-i)!} z^{k-1} \exp\left(-\frac{z}{\lambda_{el}} \frac{\mu+1}{\mu}\right) \tag{18}$$

Consequently, electron trajectories with k elastic collisions have i positions in which large angle collision can take place. We assume that the probability of k elastic collisions which occur along the trajectory reaching the depth z irrespective of the position of large angle collision is the mean value of probabilities $p_k^i(z)$

$$p_k(z) = \frac{1}{k} \sum_{i=1}^{k} p_k^i(z) \tag{19}$$

From Eqs (18) and (19), we obtain

$$p_k(z) = \frac{1}{k} \frac{1}{(\lambda_{el})^k} z^{k-1} \exp\left(-\frac{z}{\lambda_{el}} \frac{\mu+1}{\mu}\right) \sum_{i=1}^{k} \frac{1}{\mu^{k-i}} \frac{1}{(i-1)!(k-i)!} =$$

$$= \frac{1}{k} \frac{1}{(\lambda_{el})^k} \frac{1}{(k-1)!} \left(\frac{\mu+1}{\mu}\right)^{k-1} z^{k-1} \exp\left(-\frac{z}{\lambda_{el}} \frac{\mu+1}{\mu}\right) \tag{20}$$

The probability that an electron reached the depth z and left the solid without energy loss is

$$U(z) = \exp\left(-\frac{z}{\lambda_{in}} \frac{\mu+1}{\mu}\right) \tag{21}$$

http://rcin.org.pl

To calculate the penetration depth distribution function, we also need to know the angular distribution of electron directions after k collisions. This distribution is given by [20,26]

$$H_k(\cos\theta) = \frac{1}{2\pi}\sum_{l=0}^{\infty}\frac{2l+1}{2}(A_l)^k\ P_l(\cos\theta) \tag{22}$$

where $P_l(\cos\theta)$ are the Legendre polynomials, and the coefficients A_l are the expansion coefficients of the differential elastic scattering cross section into a series of Legendre polynomials

$$A_l = \frac{2\pi}{\sigma_{el}}\int_0^{\pi}\frac{d\sigma_{el}}{d\Omega}\ P_l(\cos\theta)\sin\theta\ d\theta \tag{23}$$

As shown in Fig. 3, the angle θ is related to the emission angle, α, by $\alpha = \pi - \theta$. The PDDF can be expressed then as follows

$$\xi(z,\alpha) = U(z)\sum_{k=1}^{\infty}p_k(z)\ H_k(\cos\theta) \tag{24}$$

Introducing Eqs (20) and (21) into Eq. (24), we obtain

$$\xi(z,\alpha) = \sum_{k=1}^{\infty}\frac{1}{k!\,(\lambda_{el})^k}\left(\frac{\mu+1}{\mu}\right)^{k-1}H_k(\cos\theta)\ z^{k-1}\exp\left(-\frac{z}{\lambda_t}\frac{\mu+1}{\mu}\right) \tag{25}$$

where λ_t is the total mean free path defined by

$$\lambda_t = \frac{\lambda_{el}\lambda_{in}}{\lambda_{el}+\lambda_{in}} \tag{26}$$

The PDDF can be normalized according to different rules [15]. In the present analysis, the PDDF is normalized so that the integral with respect to the depth, z, is equal to the elastic backscattering probability, $\Delta\eta$, for a small solid angle of an analyzer, $\Delta\Omega$. In that case, we have

$$\int_0^{\infty}\xi(z,\alpha)\,dz = \sum_{k=1}^{\infty}\frac{1}{k!\,(\lambda_{el})^k}\left(\frac{\mu+1}{\mu}\right)^{k-1}H_k(\cos\theta)\int_0^{\infty}z^{k-1}\exp\left(-\frac{z}{\lambda_t}\frac{\mu+1}{\mu}\right)dz \tag{27}$$

Since the integral in Eq. (27) can be solved analytically

$$\int_0^{\infty}z^{k-1}\exp\left(-\frac{z}{\lambda_t}\frac{\mu+1}{\mu}\right)dz = (k-1)!\left(\frac{\mu}{\mu+1}\right)^k(\lambda_t)^k \tag{28}$$

http://rcin.org.pl

we obtain finally

$$\int_0^\infty \xi(z,\alpha)\, dz = \frac{\mu}{\mu+1}\sum_{k=1}^{\infty}\frac{s^k}{k}\, H_k(\cos\theta) \tag{29}$$

where

$$s = \frac{\lambda_t}{\lambda_{el}} = \frac{\lambda_{in}}{\lambda_{el}+\lambda_{in}} \tag{30}$$

The expression given by Eqs (29) is identical with the elastic backscattering probability, $d\eta/d\Omega$, derived from the theory of Oswald, Kasper and Gaukler [28] and from further modifications of this theoretical model [20,26].

As follows from Eq. (2), to derive an analytical expression for the MPD for the advanced analytical model, we need to solve the following integral

$$\int_0^\infty z\,\xi(z,\alpha)\, dz = \sum_{k=1}^{\infty}\frac{1}{k!\,(\lambda_{el})^k}\left(\frac{\mu+1}{\mu}\right)^{k-1} H_k(\cos\theta)\int_0^\infty z^k \exp\left(-\frac{z}{\lambda_t}\frac{\mu+1}{\mu}\right) dz \tag{31}$$

$$= \lambda_{el}\left(\frac{\mu}{\mu+1}\right)^2 \sum_{k=1}^{\infty} s^{k+1} H_k(\cos\theta)$$

Introducing Eqs (29) and (31) into Eq. (2), we obtain

$$G = \frac{\lambda_{el}\left(\frac{\mu}{\mu+1}\right)\sum_{k=1}^{\infty} s^{k+1} H_k(\cos\theta)}{\sum_{k=1}^{\infty}\frac{s^k}{k} H_k(\cos\theta)} \tag{32}$$

An analytical expression for the ID can also be derived from the PDDF given by Eq. (25). The integral in the numerator of Eq. (3) can also be solved analytically:

$$\int_0^T \xi(z,\alpha)\, dz = \sum_{k=1}^{\infty}\frac{1}{k!\,(\lambda_{el})^k}\left(\frac{\mu+1}{\mu}\right)^{k-1} H_k(\cos\theta)\int_0^T z^{k-1} \exp\left(-\frac{z}{\lambda_t}\frac{\mu+1}{\mu}\right) dz \tag{33}$$

The integral in the right-hand side of Eq. (33) can be expressed by the incomplete gamma function, $\gamma(k,x)$ (ref. [30], p. 899). We have

$$\int_0^\infty z^{k-1} \exp\left(-\frac{z}{\lambda_t}\frac{\mu+1}{\mu}\right) dz = (\lambda_t)^k \left(\frac{\mu}{\mu+1}\right)^k \gamma\left(k, \frac{T}{\lambda_t}\frac{\mu+1}{\mu}\right) \tag{34}$$

Introducing Eq. (33) in Eq. (34), we obtain

http://rcin.org.pl

$$\int_0^T \xi(z,\alpha)\,dz = \frac{\mu}{\mu+1}\sum_{k=1}^{\infty}\frac{s^k}{k}H_k(\cos\theta)\frac{\gamma[k,\varphi(T)]}{(k-1)!} \tag{35}$$

where $\varphi(T) = \frac{T}{\lambda_t}\frac{\mu+1}{\mu}$. It is convenient to express the incomplete gamma function as a ratio with respect to the gamma function, $\Gamma(k)$ [31]

$$P[k,\varphi(T)] = \frac{\gamma[k,\varphi(T)]}{\Gamma(k)} \tag{36}$$

Since the gamma function for an integer argument is given by $\Gamma(k) = (k-1)!$, the following final equation for the ID is obtained

$$\frac{\sum_{k=1}^{\infty}\frac{s^k}{k}H_k(\cos\theta)\,P[k,\varphi(T)]}{\sum_{k=1}^{\infty}\frac{s^k}{k}\,H_k(\cos\theta)} = \frac{p_{ID}}{100} \tag{37}$$

The recommended algorithms and a complete computer code for calculations of the incomplete gamma function, $P(k,x)$, are published in ref. [31].

2.4. Angular distribution after multiple elastic collisions

As follows from Eqs (25), (32) and (37), calculations of the PDDF, the MPD and the ID from the above analytical formalism, designated here by AN, requires knowledge of the angular distribution after multiple elastic scattering, $H_k(\cos\theta)$. We note in Eq. (22) that this function is fully described by the series of coefficients A_l, i.e. the parameters of expansion of the differential elastic scattering cross sections into a series of Legendre polynomials [see Eq. (23)]. When these parameters are known, calculations of parameters describing the surface sensitivity of EPES can be very fast.

In principle, the coefficients A_l for a given element and electron energy can be calculated from Eq. (23), however this approach is inefficient in computational practice due to two reasons. First, the differential elastic scattering cross section has to be determined for a dense grid of angles to ensure a reasonable accuracy of integration. Second, a considerable number of components in the series in Eq. (22) may be needed to reach a reasonable accuracy

http://rcin.org.pl

[20]. The integrand in Eq. (23) becomes then a highly oscillating function which may considerably complicate the numerical integration. The recommended procedure takes advantage of the fact that the coefficients A_l can be expressed by an analytical formula involving only the relativistic phase shifts, δ_n^+ and δ_n^-, n = 0, 1, 2, ... [20,26]. The relevant algorithm requires calculations of the Wigner 3-j symbols $\begin{pmatrix} l & n & k \\ 0 & 0 & 0 \end{pmatrix}$ and $\begin{pmatrix} l & n & k \\ 0 & 1 & -1 \end{pmatrix}$. Details of the above approach were recently published [26]. This approach is facilitated by the fact that the needed phase shifts can be calculated from the computer code which is available in Computer Physics Communications Program Library [32,33] or obtained from the NIST database [34]. Although the recommended formalism is rather complicated, accurate values of parameters A_l can be obtained for the index l up to about 600 [26].

Fig. 4 shows examples of energy dependence of the coefficients A_l calculated for Si and Pt and for different values of the index l. We see that this dependence is a smooth function in logarithmic coordinates which makes possible an accurate interpolation. Thus, a database of coefficients A_l prepared for numerous elements for a reasonably dense grid of energies in a wide energy range would be a useful tool that considerably decreases the computing time of the PDDFs, MPDs and IDs practically without affecting their accuracy. This expectation is supported by an extensive analysis of computational procedures in calculations associated with EPES [20].

3. Results

http://rcin.org.pl

In the present analysis of the EPES sampling depth, all three theoretical models described in the previous section were used: (i) the single large-angle backscattering model (SLAB), (ii) the Monte Carlo model (MC), and (iii) the advanced theoretical model (AN).

Parameters defining the sampling depth of EPES have been calculated here for exemplary elements with atomic numbers that vary in wide range, i.e. Al, Ni, Pd and Pt. The theoretical models used the EPES applications are considered to be of a reasonable accuracy at electron energies above 200 eV [20,23,24], although the IMFPs obtained from EPES are reported for energies as low as 50 eV [2,25]. As a compromise, the energy of 100 eV was assumed as a lowest energy limit considered in the present analysis. The largest photoelectron energies observed in typical XPS spectrometers equipped with typical X-ray sources (Mg Kα and Al Kα) do not exceed 1500 eV, however due to growing interest in high energy laboratory sources, the upper limit of considered energies reaches about 5000 eV.

Theoretical models describing elastic electron backscattering require knowledge of the IMFP values [Cf. Eqs (5), (12) and (25)]. In calculations reported here, the IMFPs were taken from Tanuma et al. [4]. The differential elastic scattering cross sections, $d\sigma_{el}/d\Omega$, needed in the SLAB and MC models were directly calculated from the ELSEPA code [33]. For the AN model, the coefficients A_l were taken from the database calculated earlier [20]. Finally, the total elastic scattering cross sections, σ_{el}, needed in all three theoretical models for calculations of λ_{el}, were also calculated from the ELSEPA program [33].

3.1. Penetration depth distribution function

Since the Monte Carlo simulations are expected to provide the most reliable and accurate results, care was taken to perform calculations with a possibly good statistics. For a given element, electron energy and the experimental geometry, 8×10^7 trajectories were generated. A small solid acceptance angle of the analyzer with the half-cone angle, $\Delta\alpha$, equal to 5° has been assumed. In these calculations, precision of the elastically backscattered

http://rcin.org.pl

probability was typically below 2%. For example, the precision estimated for Pt at 2000 eV varied from 0.43% for $\alpha = 10°$ to 1.37% for $\alpha = 70°$.

The PDDFs calculated from three theoretical models for Ni and Pt in the energy range from 200 eV to 5000 eV and for the emission angle, $\alpha = 40°$, are compared in Figs 5 and 6. These functions calculated from the SLAB and the MC models differ distinctly, particularly in the region of large depths. Furthermore, the PDDFs calculated from MC simulations in some cases distinctly deviates from the exponential dependence. Ultimately, the PDDF resulting from the MC model may even exhibit a maximum, e.g. Pt at 2000 eV [see Fig 6(c)]. These results confirm the earlier published observations [15]. The PDDFs calculated from the AN model [Eq. (25)] seem to agree reasonably well with MC results in the region of depths up to about one IMFP. Furthermore, the AN model correctly predicts the presence of maximum shown in Fig. 6(c). At larger depths, the PDDFs from the AN and the MC models noticeably deviate, although in majority of cases shown in Figs 5 and 6, the PDDFs from the AN model is closer the PDDF from the MC model than the PDDF from the SLAB model.

Vertical arrows in Figs 5 and 6 indicate the depths corresponding to the MPD and the depth corresponding to a thickness a surface layer in which 95% trajectories reach maximum (the information depth corresponding to p_{ID} = 95%). The latter parameter, for brevity, is designated by ID(95). Both parameters were calculated from the MC simulations. We note that the depth of ID(95) is close to one IMFP in all cases shown in Figs 5 and 6. The MPD is smaller than the IMFP by a factor varying between 2 and 3. Thus, both parameters, MPD and ID(95) are calculated over the depth range of the PDDF in which there is a reasonable agreement between PDDFs from the MC and the AN theoretical models. Consequently, we may expect that a reasonable agreement can also be observed between the MPDs and IDs resulting from these models.

A generic function in the formalism of quantitative XPS is the emission depth distribution function (EMDDF) which describes the distribution of depths from which the signal electrons originate (ref. [1], definition 4.161). This function obtained from the MC

http://rcin.org.pl

simulations also deviates from linearity in semi-logarithmic coordinates, however this deviation typically becomes more pronounced for glancing emission angles of signal photoelectrons [35]. There are also very unusual experimental configurations in which a maximum in the EMDDF was observed (the X-ray source and an analyzer located at both sides of a thin metal foil) [36,37]. However, the maximum in the PDDF in Fig. 6(c) is observed at the medium emission angle, α, equal to 40°, and disappears at lower or higher energies. To analyze this effect more closely, the dependence of the PDDF on the emission angle for platinum at 1000 eV has been calculated from the AN theory (Fig. 7). We note that the maximum appears in the PDDFs calculated for emission angles 30°, 40° and 80°. These maxima seem to be related to the shape of the differential elastic scattering cross section. The cross section for Pt at 1000 eV exhibits two very deep minima at the scattering angles, θ, equal to 96° and 144°. These scattering angles correspond to the emission angles, α, equal to 84° and 36° since, for the considered geometry $\alpha = 180° - \theta$. Thus, there is practically no signal from atoms backscattered from atoms close to the surface at these emission angles. Any signal intensity is then due to multiple elastic collisions. In order to partially randomize the electron directions, a certain trajectory must be passed in a solid. Consequently, an increased signal intensity arises then from a depth which is at a certain distance from the surface.

3.2. Mean penetration depth

The MPDs for considered elements in the energy range from 100 eV to 5000 eV are shown in Figs 8-11. These parameters for the SLAB and AN models (G_{SLAB} and G_{AN}) were calculated from Eqs (6) and (32), respectively. The MPD from the MC calculations (G_{MC}) was estimated by introducing the PDDF from Eq. (13) into the defining formula [Eq. (2)].

In practically all cases, the MPDs calculated from the AN and MC models agree reasonably well, while the MPD obtained from the SLAB model considerably deviates. The

http://rcin.org.pl

only exception is observed in the region of high energies for Al (1000 eV, 2000 eV and 5000 eV) and Ni (5000 eV). In these cases, the angular dependence of MPDs obtained from the three theoretical models is similar. The MPDs, G_{SLAB}, is always a monotonically decreasing function of the emission angle, α. More accurate models, the AN and MC models, provide the angular dependence that frequently exhibit a maximum, or even two maxima (e.g. MPD for Pt at 500 eV). The shape of angular dependence of the MPD and the position of the maximum or maxima are in a very good agreement.

Let us quantify the differences between MPDs shown in Figs 8-11. To evaluate the reliability of the AN model, the following percentage deviations from were calculated for a given emission angle:

$$\Delta G_{MC} = 100 \frac{G_{AN} - G_{MC}}{G_{AN}} \tag{38}$$

Furthermore, let us evaluate comparison of both analytical models described here. We have then

$$\Delta G_{SLAB} = 100 \frac{G_{AN} - G_{SLAM}}{G_{AN}} \tag{39}$$

Examples of these results are shown in Figs 12 and 13. Generally, the percentage differences between the MPDs from the MC calculations and the from the AN model do not exceed about 10%. More pronounced differences are observed for the largest emission angle considered ($\alpha = 80°$) or for the lowest energy (100 eV). As expected, the percentage differences ΔG_{SLAM} are much larger than ΔG_{MC}. They may even reach 80% (see e.g. Ni at 200 eV). Let us average the percentage deviations between the MC and the AN models over the considered angular range according to the rule

$$< \Delta G_{MC} > = \frac{1}{n_\alpha} \sum_{i=1}^{n_\alpha} \left| \Delta G_{MC}^{(i)} \right| \tag{40}$$

where n_α is the number of emission angles. Similarly, we use the following averaging procedure for the AN and the SLAB models:

http://rcin.org.pl

$$< \Delta G_{SLAB} > = \frac{1}{n_\alpha} \sum_{i=1}^{n_\alpha} \left| \Delta G_{SLAB}^{(i)} \right| \quad (41)$$

Results of calculations are compiled in Table 1. We see that the MPDs from the MC and the AN models agree very well. The mean percentage differences $< \Delta G_{MC} >$ are typically below 5%. Distinctly larger values were found only for the lowest energy. Since applications of the EPES method is recommended for energies above 200 eV, the values of $< \Delta G_{MC} >$ were further averaged over energy range from 200 eV to 5000 eV. As shown in Table 1, these averages vary from 3.24% to 4.68% which proves an excellent agreement between the MC and the AN theoretical models. In fact, a similar agreement was found recently in comparison of ratios of elastic backscattering probabilities resulting from Monte Carlo simulations and from an analytical formalism based on similar assumptions as the presently considered AN model (Table 3 of ref. [20]).

The mean percentage differences between the AN and SLAB analytical models, $< \Delta G_{SLAM} >$, are larger than $< \Delta G_{MC} >$ in majority of cases; they even reach 38%. For consistency, the mean percentage differences, $< \Delta G_{SLAM} >$, are further averaged over the energy range from 200 eV to 5000 eV. The averaged values reach 26.12% for Pt; thus they are considerably larger than the same averaged differences between the AN and the MC models. Consequently, the SLAB model cannot be recommended for estimation of the MPDs of EPES.

3.3. Information depth

The ID due to backscattered electrons, *T*, was calculated for three routinely selected percentages p_{ID}: $p_{ID} = 90\%$, $p_{ID} = 95\%$ and $p_{ID} = 99\%$. The IDs due to the SLAB model were calculated from Eq. (7). For the AN model, calculations were more complicated since the nonlinear equation [Eq (37)] had to be solved. However, these calculations were relatively fast. Finally, the IDs corresponding to the MC model were obtained by solving the defining equation [Eq. (3)] after introducing the PDDF function estimated from the MC simulations

http://rcin.org.pl

[Eqs (12) and (13)]. Exemplary results for Al and Ni at 500 eV are shown in Fig 14. We note that the shape of the emission angle dependence of the IDs is very similar to the shape of the MPDs. However, the agreement between IDs form the MC and the AN models is not so good as in the case of the corresponding MPDs [see Figs 8(c) and 9(c)]. Generally, the IDs resulting from the AN model are overestimated with exception of the region of the largest emission angles. Pronounced deviations are observed for the largest percentage, p_{ID}, i.e. $p_{ID} = 99\%$. This difference can be partially ascribed to the fact that 99% of the signal intensity is comparable with precision of the backscattered current estimated from the Monte Carlo simulations (typically between 0.5% and 1.5%).

In Figs 15 and 16, the emission angle and energy dependence of the ID for the signal percentage $p_{ID} = 95\%$, *T*(95), is shown. These results were obtained for Pd and Pt using three theoretical models (AN, MC and SLAB). As in the case of Al and Ni (Fig. 14), we observe reasonably good agreement between IDs obtained from the AN and MC theoretical model, although the difference seems to be larger as in the case of the MPDs. The shape of angular dependence of IDs is very close to the angular dependence of the MPDs shown in Figs 10 and 11. Except for the emission angle 80°, the IDs obtained from the AN theoretical model are noticeably overestimated. As in the case of MPDs shown in Figs 8-11, the IDs from the SLAB model have a different shape of the angular dependence (a monotonic decrease) and considerably deviates from the IDs calculated from the AN and MC models.

Let us determine the mean percentage deviations between the AN and MC models and also between the two analytical models (AN and SLAB). They were calculated from similar criterions as in the case of MPDs [see Eqs (38) – (39)]

$$< \Delta T(p_{ID})_{MC} > = \frac{1}{n_\alpha}\sum_{i=1}^{n_\alpha}\left|\Delta T(p_{ID})_{MC}^{(i)}\right| \tag{42}$$

$$< \Delta T(p_{ID})_{SLAB} > = \frac{1}{n_\alpha}\sum_{i=1}^{n_\alpha}\left|\Delta T(p_{ID})_{SLAB}^{(i)}\right| \tag{43}$$

where $\Delta T(p_{ID})_{MC}$ and $\Delta T(p_{ID})_{SLAB}$ are percentage differences given by

http://rcin.org.pl

$$\Delta T(p_{ID})_{MC} = 100\frac{T(p_{ID})_{AN} - T(p_{ID})_{MC}}{T(p_{ID})_{AN}} \quad (44)$$

$$\Delta T(p_{ID})_{SLAB} = 100\frac{T(p_{ID})_{AN} - T(p_{ID})_{SLAB}}{T(p_{ID})_{AN}} \quad (45)$$

The mean percentage deviations were calculated for percentages p_{ID} equal to 90%, 95% and 99%. Results are compiled in Tables 2 - 4. As expected, the mean percentage differences between the AN and MC models, $\Delta T(p_{ID})_{MC}$, are on average about twice larger as in the case of the MPDs. For $p_{ID} = 90\%$ and $p_{ID} = 95\%$ they are very close (Tables 2 and 3). The total mean averaged over the energy range from 200 eV to 5000 eV varies between 7.21% and 8.64%. Slightly more pronounced mean percentage differences are found for $p_{ID} = 99\%$ (Table 4). The total mean reaches then 10.04%. As expected, the mean percentage deviations between the SLAB and the AN models, $\Delta T(p_{ID})_{SLAB}$ are much larger. The total mean reaches 24%. Thus, we may state that the AN model is a convenient and reasonably accurate tool that can be used for estimation of the sampling dept of EPES.

4. Discussion and conclusions

An intriguing feature that is observed in the emission angle dependence of MPDs and IDs is presence of a maximum, or even maxima, that appear for all elements considered here at certain energies. This effect was initially reported for Au at 1000 eV and tentatively related to the shape of the differential elastic scattering cross section [15]. As follows from the AN model outlined in Fig. 3, the elastic backscattering event is dominated by a single large angle elastic collision. Thus, the minimum of in the differential elastic scattering cross section leads to a minimum in the emission angle dependence of the elastic backscattering probability. Thus effect has been visualized experimentally for Au at energies of 500 eV and 800 eV [18]. The minima in the signal intensities seem to be correlated with maxima observed in the angular dependence of MPDs and IDs.

http://rcin.org.pl

Let us consider here this effect more closely. We select for analysis an element and energies for which two minima were found, i.e. Pt at 200 eV and 500 eV [Cf. Figs 11(b) and 11(c)]. Fig. 17 compares the differential elastic scattering cross sections with the signal intensity, and the corresponding parameters defining the sampling depth. In the lowest panel, the differential elastic scattering cross sections in the large scattering angle range is shown. The emission angle, α, is related to the scattering angle θ by $\alpha = 180° - \theta$ (see Fig. 3). Positions of minima correspond to minima in the emission angle dependence of the signal intensity shown in the middle panel. The AN model was used in these calculations. However, at the same angles, we observe maxima in the emission angle dependence of the MPDs and IDs. The origin of this effect seems to be similar as in the case of maxima in PDDFs. If an analyzer in positioned in vicinity of the minimum in the differential elastic scattering cross section, backscattered electrons due to large-angle scattering event practically do not contribute to the signal intensity. The signal is dominated by electrons with randomized directions. To be partially randomized due to small scattering angle events, the trajectory of an electron must be longer compared with a situation in which the large-angle scattering is dominating. As follows from Fig. 3, the trajectory length and the depth are related; a longer trajectory reaches a larger depth.

Important information can be obtained from values of maxima in the angular dependence of the MDPs and IDs. Let us express the sampling depth as a following ratio

$$R_{ID}(p_{ID}) = \frac{T(p_{ID})}{\lambda_{in}} \tag{46}$$

These ratios were calculated for all elements and energies in the angular range $0 \le \alpha \le 85°$ and the maximum value, $\max_{0 \le \alpha \le 85°} R_{ID}(p_{ID})$, was determined. The AN theoretical model was used in this analysis. Results are shown in Fig. 18. As expected, the largest ratios were obtained for the percentage, p_{ID} = 99%; they are shown in the upper panel of Fig. 18. The largest values in this panel are equal to 2.39 and 2.37 for Al and Ni at 5000 eV, respectively. From this observation, we can estimate the minimum thickness of an overlayer that is needed

http://rcin.org.pl

for the EPES measurements, e.g. measurement of the IMFPs for an overlayer material. The value of 2.37 can be overestimated due to two reasons. First, we analyzed here all the angular range varying from $\alpha = 0^{o}$ to $\alpha = 85^{o}$ while the range of angles recommended for EPES is more narrow, e.g. the range recommended in ref. [26] is diminished to $35° \le \alpha \le 74°$. Second, the AN model tends to overestimate the ID as compared to the MC model (see Figs 15 and 16). However, the AN model is very convenient to use in calculations of the maximum ID due to a large speed of computations. On the other hand, we analyzed here only four elemental solids. If this analysis is extended to other solids, larger maximum values can be obtained. For safety, let us tentatively assume that the recommended minimum thickness of an overlayer for the EPES measurements is equal to 3 IMFPs. For example, the largest IMFP values used here is 8.021 nm for Al at 5000 eV [4]. Thus, the minimum overlayer thickness postulated here for EPES measurements is close to 24 nm. The IMFPs for these estimations for elements can be taken from Tanuma et al. [4]. For compounds, the TPP-2M predictive formula is recommended [7].

Main objective of the present work was to derive a fast and accurate algorithm for calculating parameters describing the sampling depth of EPES, i.e. PDDF, MPD and ID. The AN theoretical model fulfils these requirements. It should be mentioned, however, that the series in Eqs (25), (32) and (37) is slowly convergent. To accelerate the convergence, one can take advantage of the fact that after a certain number of elastic collisions, k_0, the distribution of electron directions becomes close to uniform in space, i.e. the distribution $H_k(\cos\theta)$ after randomization reaches the constant value $1/(4\pi)$. Let us consider the series in denominator of Eqs (32) and (37). We have

$$\sum_{k=1}^{\infty} \frac{s^k}{k} H_k(\cos\theta) = \sum_{k=1}^{k_0-1} \frac{s^k}{k} H_k(\cos\theta) + \frac{1}{4\pi} \sum_{k=k_0}^{\infty} \frac{s^k}{k} = \tag{47}$$

$$= \sum_{k=1}^{k_0-1} \frac{s^k}{k} H_k(\cos\theta) - \frac{1}{4\pi} \left[\ln(1-s) + \sum_{k=1}^{k_0-1} \frac{s^k}{k} \right]$$

http://rcin.org.pl

since $= \sum_{k=1}^{\infty} \frac{s^k}{k} = -\ln(1-s)$. Another condition for fast performance of the AN formalism is a convenient access to the database of the parameters A_l since an algorithm for calculating these parameters is rather involved [20,26], and such calculations may require a considerable computer time. Such a database is presently prepared for publication [38].

Analysis of the AN model was limited here to elemental solids. However, this model can be readily generalized to compounds. Let us consider a compound consisting of m elements; and let us denote the atom fraction of i-th element by x_i. It has been shown that the parameter A_l to be used in the AN formalism for compounds is given by [20]

$$A_l = \sum_{i=1}^{m} p_i A_l^{(i)} \tag{48}$$

where $A_l^{(i)}$ is the A_l parameter for the i-th element, and p_i is the probability that the elastic scattering event occurs on the i-th atomic species

$$p_i = \frac{x_i \sigma_{el}^{(i)}}{\sum_{j=1}^{m} x_j \sigma_{el}^{(j)}} \tag{49}$$

Thus, to calculate the distribution of electron directions after k collisions, $H_k(\cos\theta)$, we replace the expression $(A_l)^k$ in Eq. (22) by $\left(\sum_{i=1}^{m} p_i A_l^{(i)} \right)^k$. For calculations of the PDDF, MPD and ID for compounds [Eqs ((25), (32) and (37)], we also need to know the elastic mean free path, λ_{el}. The following expression has been proposed [20]

$$\lambda_{el} = \frac{1}{N_A \rho} \frac{\sum_{i=1}^{m} x_i M_i}{\sum_{i=1}^{m} x_i \sigma_{el}^{(i)}} \quad , \tag{50}$$

where ρ is the density of a compound and M_i is the corresponding atomic mass.

It would certainly be of interest to compare the presently proposed criteria of the sampling depth with experimental observations. Although no simple and universal procedure for such comparisons seems to be available, an experimental approach outlined below can be

http://rcin.org.pl

useful for selected solids. Let us consider an experiment in which the elastic backscattering probability is measured for an overlayer deposited in consecutive increments on a substrate. The pair overlayer-substrate and the experimental configuration should be selected so that this probability varies considerably with the overlayer thickness. A good example of such system is the Au overlayer deposited on the Ni substrate [18,19]. Let us denote by $\eta_t(\Delta\Omega)$ the elastic backscattering probability for an overlayer of thickness *t*, and by $\eta_0(\Delta\Omega)$ the elastic backscattering probability for an uncovered substrate. An example of the overlayer thickness dependence of the ratio,

$$R_\eta(t) = \frac{\eta_t(\Delta\Omega)}{\eta_0(\Delta\Omega)}, \tag{51}$$

measured for the Au/Ni system at energy of 500 eV, taken from ref. [19], is shown in Fig. 19. We see that this ratio varies by the factor of three. The upper vertical lines indicate values of the ID calculated from the advanced theoretical model [Eq. (37)]. Values of ID(90), ID(95) and ID(99) (equal to 1.021 nm, 1.268 nm and 1.835 nm, respectively) are located in the region of thicknesses in which presence of the substrate does not have any effect on measured relative intensities, $R_\eta(t)$.

On close inspection of Fig. 19, one can propose a crude estimation an overlayer thickness corresponding to the ID. It has been found [19] that the overlayer thickness dependence of $R_\eta(t)$ can be well approximated by the expression

$$R_\eta(t) = R_\eta(\infty) + [1 - R_\eta(\infty)]\exp(-k\,t) \tag{52}$$

where $R_\eta(\infty)$ is the relative intensity corresponding to large overlayer thicknesses, and *k* is the fitted constant. Let us assume that the relative intensity becomes practically constant if it does not deviate from $R_\eta(\infty)$ by more than several percent, e.g. $\Delta p = 10\%$

$$\Delta p = 100\frac{|R_\eta(t) - R_\eta(\infty)|}{R_\eta(\infty)} = 100 - p_{ID} \tag{53}$$

http://rcin.org.pl

Let us calculate the thickness t for the three routinely used percentages, p_{ID}. From Eq. (52) and (53), the following relation can be derived.

$$t(p_{ID}) = -\frac{1}{k}\ln\left[\frac{100-p_{ID}}{100}\,\frac{R_{\eta}(\infty)}{1-R_{\eta}(\infty)}\right] \tag{54}$$

The thicknesses $t(p_{ID})$ calculated from Eq. (54) are indicated by vertical lines in the lower part of Fig. 19 [$t(90) = 0.905$ nm, $t(95) = 1.105$ nm, $t(99) = 1.570$ nm]. Although these values differ somewhat from the theoretical IDs, we may tentatively state that a given thickness $t(p_{ID})$ can be a conside3red as a reasonable experimental measure of the sampling depth of EPES measurements. We note that the presently proposed criterion for safe overlayer thickness, equal to three IMFPs, provides the value 3×0.835 nm = 2.505 nm which is located in the horizontal part of the plot shown in Fig. 19.

In conclusion, elastic peak electron spectroscopy is a convenient tool for analytical applications in studies of overlayers with thickness in the range of nanometers. Determination of the IMFPs for overlayers is an application of a particular importance. It has been recently proved that the analytical formalism based on the same assumptions as in the present work leads to the IMFPs of similar accuracy as Monte Carlo algorithms [20]. For the energy range from 200 eV to 5000 eV, the percentage deviation between the IMFPs from the MC and the AN algorithms averaged over 13 elements was equal to 3.09%. In the present work, the mean percentage deviation between the MPDs from the MC and AN models varies from 3.24% to 4.68%. The mean percentage differences between IDs from two theoretical models are about twice larger. The emission angle dependence of the ID is shown to have a complicated structure for some elements and energies which are shown to be correlated with the shape of the differential elastic scattering cross section. The maximum value of the ID is shown not to exceed a layer with thickness of three IMFPs which leads to a convenient guidance of the minimum overlayer thickness suitable for EPES measurements.

http://rcin.org.pl

References

[1] ISO 18115-1, Surface Chemical Analysis – Vocabulary, Part 1 – General Terms and Terms Used in Spectroscopy, International Organization for Standardization, Geneva, 2013; definition 4.243.

[2] C. J. Powell, A. Jablonski, Evaluation of calculated and measured electron inelastic mean free paths near solid surfaces, J. Phys. Chem. Ref. Data 28 (1999) 19-62.

[3] S. Tanuma, C. J. Powell, D. R. Penn, Calculations of electron inelastic mean free paths. II. data for 27 elements over the 50-2000 eV range, Surface Interface Anal. 17 (1991) 911-926.

[4] S. Tanuma, C. J. Powell, D. R. Penn, Calculations of electron inelastic mean free paths. IX. Data for 41 elemental solids over the 50 eV to 30 keV range, Surface Interface Anal. 43 (2011) 689-713.

[5] H. Shinotsuka, S. Tanuma, C. J. Powell, D. R. Penn, Calculations of electron inelastic mean free paths. X. Data for 41 elemental solids over the 50 to 200 keV range with the relativistic full Penn algorithm, Surface Interface Anal. 47 (2015) 871-888.

[6] S. Tanuma, C. J. Powell, D. R. Penn, Calculations of electron inelastic mean free paths. III. Data for 15 inorganic compounds over the 50-2000 eV range, Surface Interface Anal. 17 (1991) 927-939.

[7] S. Tanuma, C. J. Powell, D. R. Penn, Calculations of electron inelastic mean free paths. V. Data for 14 organic compounds over the 50-2000 eV range, Surface Interface Anal. 21 (1994) 165-176.

[8] C. J. Powell, A. Jablonski, NIST Electron Inelastic-Mean-Free-Path Database, Version 1.2, Standard Reference Data Program Database 71, US Department of Commerce, National Institute of Standards and Technology, Gaithersburg, MD (2010); web address: http://www.nist.gov/srd/nist71.cfm

[9] Y. F. Chen, P. Su, C. M. Kwei, C. J. Tung, Influence of surface excitations on

http://rcin.org.pl

electrons elastically backscattered from copper and silver surfaces, Phys. Rev. B50 (1994) 17547-17555.

[10] S. Tanuma, S. Ichimura, K. Goto, Estimation of surface excitation correction factor for 200-5000 eV in Ni from absolute elastic scattering electron spectroscopy, Surface Interface Anal. 30 (2000) 212-216.

[11] Y. F. Chen, Surface effects on angular distributions in X-ray-photoelectron spectroscopy, Surface Sci. 519 (2002) 115-124.

[12] W. S. M. Werner, W. Smekal, C. Tomastik, H. Störi, Surface excitation probability of medium energy electrons in metals and semiconductors, Surface Sci. 486 (2001) L461-L466.

[13] W. S. M. Werner, L. Kover, S. Egri, J. Toth, D. Varga, Measurement of the surface excitation probability of medium energy electrons reflected from Si, Ni, Ge and Ag surfaces, Surface Sci. 585 (2005) 85-94.

[14] A. Jablonski, J. Zemek, Angle resolved elastic peak electron spectroscopy: Role of surface excitations, Surface Sci. 601 (2007) 3409-3420.

[15] A. Jablonski, C. J. Powell, Information depth for elastic-peak electron spectroscopy, Surface Sci. 551 (2004) 106-124.

[16] A. Jablonski, J. Zemek, Angle-resolved elastic-peak electron spectroscopy: Solid-state effects, Surface Sci. 600 (2006) 4464-4474.

[17] L. Zommer, A. Jablonski, EPES sampling depth paradox for overlayer/substrate system, J. Electron Spectosc. Relat. Phenom. 150 (2006) 56-61.

[18] A. Jablonski, H. S. Hansen, C. Jansson, S. Tougaard, Elastic electron backscattering from surfaces with overlayers, Phys. Rev. B45 (1992) 3694-3702.

[19] A. Jablonski, J. Zemek, P. Jiricek, Elastic electron backscattering from overlayer/substrate systems, Surface Interface Anal. 31 (2001) 825-834.

[20] A. Jablonski, Analytical theory of elastic electron backscattering from elements, alloys and compounds: Comparison with experimental data, J. Electron Spectrosc. Relat.

http://rcin.org.pl

Phenom. 206 (2016) 24-45.

[21] A. Jablonski, C. Jansson, S. Tougaard, Elastic backscattering from surfaces. Prediction of maximum intensity, Phys. Rev. B47 (1993) 7420-7430.

[22] A. Jablonski, J. Zemek, Maximum probability of elastic electron backscattering from amorphous and polycrystalline solids, Surface Sci. 347 (1996) 207-214.

[23] W. S. M. Werner, C. Tomastic, T. Cabela, G. Richter, H. Störi, Electron inelastic mean free path measured by elastic peak electron spectroscopy for 24 solids between 50 and 3400 eV, Surface Sci. 470 (2000) L123-L128.

[24] W. S. M. Werner, C. Tomastic, T. Cabela, G. Richter, H. Störi, Elastic electron reflection for determination of the inelastic mean free path of medium energy electrons in 24 elemental solids for energies between 50 and 3400 eV, J. Electron Spectrosc. Relat. Phenom. 113 (2001) 127-135.

[25] S. Tanuma, T. Shiratori, T. Kimura, K. Goto, S. Ichimura, C. J. Powell, Experimental determination of electron inelastic mean free paths in 13 elemental solids in the 50 to 5000 eV energy range by elastic-peak electron spectroscopy, Surface Interface Anal. 37 (2005) 833-845.

[26] A. Jablonski, Angular distribution of elastic electron backscattering from surfaces: determination of the electron inelastic mean free path, J. Phys. D: Appl. Phys. 47 (2014) 055301.

[27] W. S. M. Werner, Trajectory reversal approach for electron backscattering from solid surfaces, Phys. Rev. B71 (2005) 115415.

[28] R. Oswald, E. Kasper, K. H. Gaukler, A multiple scattering theory of elastic electron backscattering from amorphous surfaces, J. Electron Spectrosc. Relat. Phenom. 61 (1993) 251-274.

[29] H. C. Tijms, Stochastic models. An algorithmic approach, J. Wiley, Chichester, 1994, p. 347.

[30] I. S. Gradshteyn, I. M. Ryzhik, Table of integrals, series, and products, 7th edition,

http://rcin.org.pl

Elsevier, Amsterdam, 2007.

[31] W. H. Press, S. A. Teukolsky, W. T. Vetterling, B. P. Flannery, Numerical Recipes. The Art of Scientific Computing, Cambridge University Press, Cambridge (2007), pp 259-263.

[32] F. Salvat, A. Jablonski, C. J. Powell, ELSEPA - Dirac partial-wave calculation of elastic scattering of electrons and positrons by atoms, positive ions and molecules, Comput. Phys. Commun. 165 (2005) 157-190.

[33] Computer Physics Communications Program Library; Programs in Physics and Physical Chemistry; web address: http://cpc.cs.qub.ac.uk/cpc/summaries/ADUS

[34] A. Jablonski, F. Salvat, C. J. Powell, NIST Electron Elastic-Scattering Cross-Section Database, Version 3.2, Standard Reference Data Program Database 64, U.S. Department of Commerce, National Institute of Standards and Technology, Gaithersburg, MD (2010); web address: http://www.nist.gov/srd/nist64.cfm

[35] A. Jablonski, Emission depth distribution function for photoelectrons emitted by laboratory hard X-ray radiation sources, J. Electron Spectrosc. Relat. Phenom. 195 (2014) 26-42

[36] J. Zemek, S. Hucek, A. Jablonski, I. S. Tilinin, Escape probability of s-photoelectrons leaving aluminium and copper oxides, Surface Interface Anal. 26 (1998) 182-187.

[37] J. Zemek, P. Jiricek, S. Hucek, A. Jablonski, B. Lesiak, Escape probability of photoelectrons from silver sulphide, Surface Sci. 473 (2001) 8-16.

[38] A. Jablonski, to be published.

cc BY NC

http://rcin.org.pl

Table 1. Mean percentage deviations, $<\Delta G_{MC}>$ and $<\Delta G_{SLAB}>$, calculated from Eqs (40) and (41), respectively. The total mean values are obtained by averaging the mean percentage deviations over the energy range from 200 eV to 5000 eV, i.e. over the range of validity of the EPES method.

Energy (eV)	Mean percentage deviation, $<\Delta G_{MC}>$ (%)			
	Al	Ni	Pd	Pt
100	2.10	8.73	10.17	17.68
200	1.87	5.79	6.32	5.06
500	2.96	3.10	4.12	7.63
1000	4.31	2.98	3.23	3.41
2000	4.42	4.47	2.31	3.99
5000	2.63	5.37	4.10	3.29
Total mean:	3.24	4.34	4.02	4.68

Energy (eV)	Mean percentage deviation $<\Delta G_{SLAB}>$ (%)			
	Al	Ni	Pd	Pt
100	31.93	33.07	32.26	10.44
200	22.90	37.83	30.20	19.99
500	10.42	31.82	31.50	27.04
1000	0.98	21.00	27.95	35.17
2000	3.68	8.11	17.24	29.89
5000	3.87	3.41	4.82	18.50
Total mean:	8.37	20.43	22.34	26.12

cc BY NC
http://rcin.org.pl

Table 2. Mean percentage deviations, $<\Delta T(90)_{MC}>$ and $<\Delta T_{SLAB}(90)>$, calculated from Eqs (42) and (43), respectively. The total mean values are obtained by averaging the mean percentage deviations over the energy range from 200 eV to 5000 eV.

Energy (eV)	Mean percentage deviation $<\Delta T(90)_{MC}>$, (%)			
	Al	Ni	Pd	Pt
100	5.54	14.33	13.83	22.29
200	5.32	9.91	11.16	9.78
500	7.07	6.44	7.93	11.52
1000	8.68	7.34	6.22	7.37
2000	8.37	9.20	6.24	7.64
5000	6.63	10.30	8.38	6.87
Total mean:	7.21	8.64	7.98	8.64

Energy (eV)	Mean percentage deviation $<\Delta T(90)_{SLAB}>$, (%)			
	Al	Ni	Pd	Pt
100	30.70	31.30	29.56	6.04
200	22.70	36.72	26.99	17.12
500	10.25	30.59	29.19	23.95
1000	0.99	20.73	25.81	33.58
2000	3.66	7.94	16.92	27.44
5000	3.91	3.33	4.70	17.71
Total mean:	8.30	19.86	20.72	23.96

http://rcin.org.pl

Table 3. Mean percentage deviations, $<\Delta T(95)_{MC}>$ and $<\Delta T_{SLAB}(95)>$, calculated from Eqs (42) and (43), respectively. The total mean values are obtained by averaging the mean percentage deviations over the energy range from 200 eV to 5000 eV.

Energy (eV)	Mean percentage deviation $<\Delta T(95)_{MC}>$ (%)			
	Al	Ni	Pd	Pt
100	6.28	15.08	13.78	21.81
200	5.60	9.51	11.77	10.06
500	7.16	6.55	7.39	11.56
1000	8.57	7.37	5.49	7.10
2000	8.54	9.51	5.94	6.74
5000	6.30	10.50	8.37	6.57
Total mean	7.24	8.69	7.79	8.41

Energy (eV)	Mean percentage deviation, $<\Delta T(95)_{SLAB}>$, (%)			
	Al	Ni	Pd	Pt
100	29.48	30.02	28.01	4.35
200	22.30	36.12	24.60	14.45
500	10.07	29.46	27.78	21.86
1000	1.13	20.15	24.25	32.44
2000	3.49	7.85	16.47	25.97
5000	3.86	3.06	4.65	16.80
Total mean	8.17	19.33	19.55	22.30

http://rcin.org.pl

Table 4. Mean percentage deviations, $<\Delta T(99)_{MC}>$ and $<\Delta T_{SLAB}(99)>$, calculated from Eqs (42) and (43), respectively. The total mean values are obtained by averaging the mean percentage deviations over the energy range from 200 eV to 5000 eV.

Energy (eV)	Mean percentage deviation, $<\Delta T(99)_{MC}>$, (%)			
	Al	Ni	Pd	Pt
100	8.47	16.81	15.57	20.78
200	7.36	10.59	13.89	12.15
500	7.62	8.71	8.05	12.75
1000	8.52	9.60	7.44	8.88
2000	8.38	10.19	7.65	7.89
5000	5.90	10.43	8.56	8.54
Total mean:	7.56	9.90	9.12	10.04

Energy (eV)	Mean percentage deviation $<\Delta T(99)_{SLAB}>$ (%)			
	Al	Ni	Pd	Pt
100	27.12	27.05	25.16	3.17
200	21.17	33.99	21.34	10.23
500	9.68	27.65	25.61	19.29
1000	1.41	18.83	21.59	30.03
2000	3.11	7.68	15.69	23.74
5000	3.75	2.44	4.58	15.47
Total mean:	7.82	18.12	17.76	19.75

http://rcin.org.pl

Figure Captions

Fig. 1. Scheme of trajectory of elastically backscattered electron illustrating the single large-angle backscattering model (SLAB).

Fig. 2. Scheme of trajectory of elastically backscattered electron illustrating the strategy of Monte Carlo calculations (MC).

Fig. 3. Example of an electron trajectory illustrating assumptions of the analytical formalism (AN) and the notation used.

Fig. 4. 3D plots of the dependence of parameters A_l on energy and the index l varying in the range $0 \le l \le 50$. (a) Aluminium; (b) platinum.

Fig. 5. Penetration depth distribution function calculated for nickel assuming the emission angle, α, equal to 40°. Depth is expressed in terms of the IMFP for a particular electron energy. Solid line: the AN formalism; dotted line: the SLAB model; circles: the Monte Carlo calculations. Vertical arrows indicate the depth corresponding to the mean penetration depth and the 95% information depth. (a) Energy of 200 eV; (b) 500 eV; (c) 2000 eV; (d) 5000 eV.

Fig. 6.The same as Fig 5 except for platinum.

Fig. 7. Dependence of the PDDF the on the emission angle, α, calculated from the AN model for platinum and energy of 1000 eV. Depth is expressed in terms of the IMFP.

Fig 8. Dependence of the mean penetration depth on the emission angle, α, calculated for aluminium. Solid line: the AN formalism; dotted line: the SLAB model; circles: the Monte Carlo calculations. (a) Energy of 100 eV; (b) 200 eV; (c) 500 eV; (d) 1000 eV; (e) 2000 eV; (f) 5000 eV.

Fig. 9.The same as Fig 8 except for nickel.

Fig. 10.The same as Fig 8 except for palladium.

Fig. 11.The same as Fig 8 except for platinum.

Fig. 12. Percentage differences between MPDs for nickel obtained from considered theoretical models. Solid line: difference between the AN and the SLAB models [ΔG_{SLAB} , Eq.

http://rcin.org.pl

(39)]; circles: difference between the AN and the MC models [ΔG_{MC}, Eq. (38)]. (a) Energy of 100 eV; (b) 200 eV; (c) 500 eV; (d) 1000 eV; (e) 2000 eV; (f) 5000 eV.

Fig. 13. The same as Fig. 12 except for platinum.

Fig. 14. Dependence of the information depth on the emission angle, α, calculated for energy of 500 eV and the three percentages, p_{ID}, considered here ($p_{ID} = 90\%$, $p_{ID} = 95\%$ and $p_{ID} = 99\%$). Solid line: the AN model; symbols: the MC calculations. The angular dependence of the MPD is also show here for comparison (dotted line). Horizontal line indicates the IMFP value. (a) aluminium; (b) nickel.

Fig. 15. Dependence of the ID(95) on the emission angle, α, calculated for palladium. Solid line: the AN formalism; dotted line: the SLAB model; circles: the Monte Carlo calculations. (a) Energy of 100 eV; (b) 200 eV; (c) 500 eV; (d) 1000 eV; (e) 2000 eV; (f) 5000 eV.

Fig. 16. The same as Fig. 15 except for platinum.

Fig. 17. (Upper panel) Angular dependence of MPD (solid line) and ID(95) (dotted line) calculated from the AN model for platinum. (Middle panel) The corresponding angular dependence of the backscattered intensity. (Lower panel) The differential elastic scattering cross section plotted in coordinates $d\sigma_{el} / d\Omega$ versus $\alpha = 180° - \theta$. Vertical lines indicate positions of minima in the DCS.

Fig. 18. Value of maximum in the angular dependence of the ID(p_{ID}) expressed in units of the IMFP as a function of energy .Circles: aluminium; triangles: nickel; squares: palladium; diamonds: platinum. (a) Percentage of signal intensity, $p_{ID} = 99\%$; (b) $p_{ID} = 95\%$; (c) $p_{ID} =$ 90%.

Fig. 19. Dependence of the relative elastic backscattering probability of 500 eV electrons, $R_\eta(t)$, on thickness of the Au overlayer deposited on the Ni substrate. Triangles: the experimental data; solid line: the fitted function [Eq. (52)]. The vertical lines indicate positions of the information depths [ID(90), ID(95) and ID(99)], and thicknesses at which the influence of the substrate starts to be negligible [t(90), t(95) and t(99); see text for details].

http://rcin.org.pl

http://rcin.org.pl

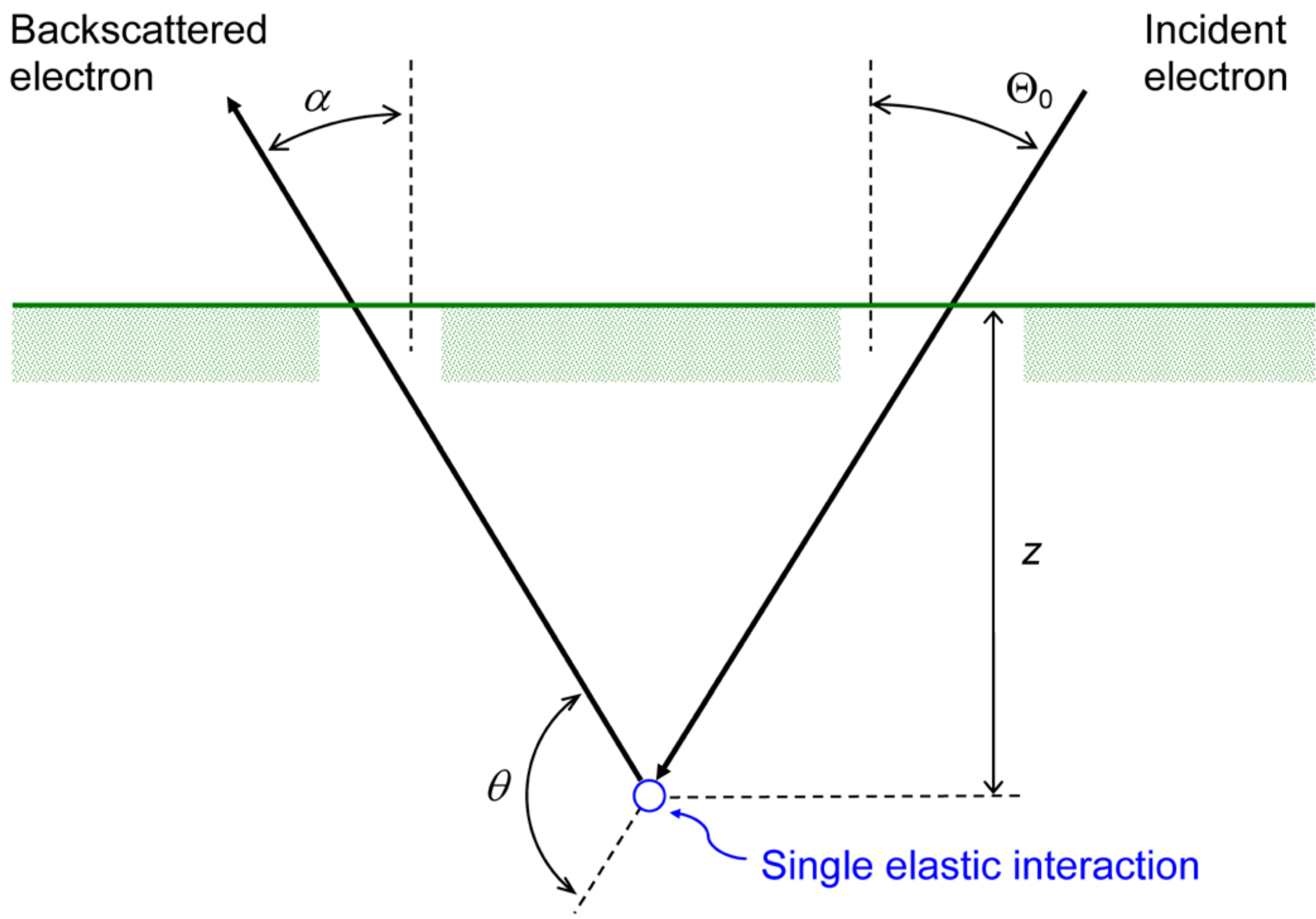

Fig. 1

http://rcin.org.pl

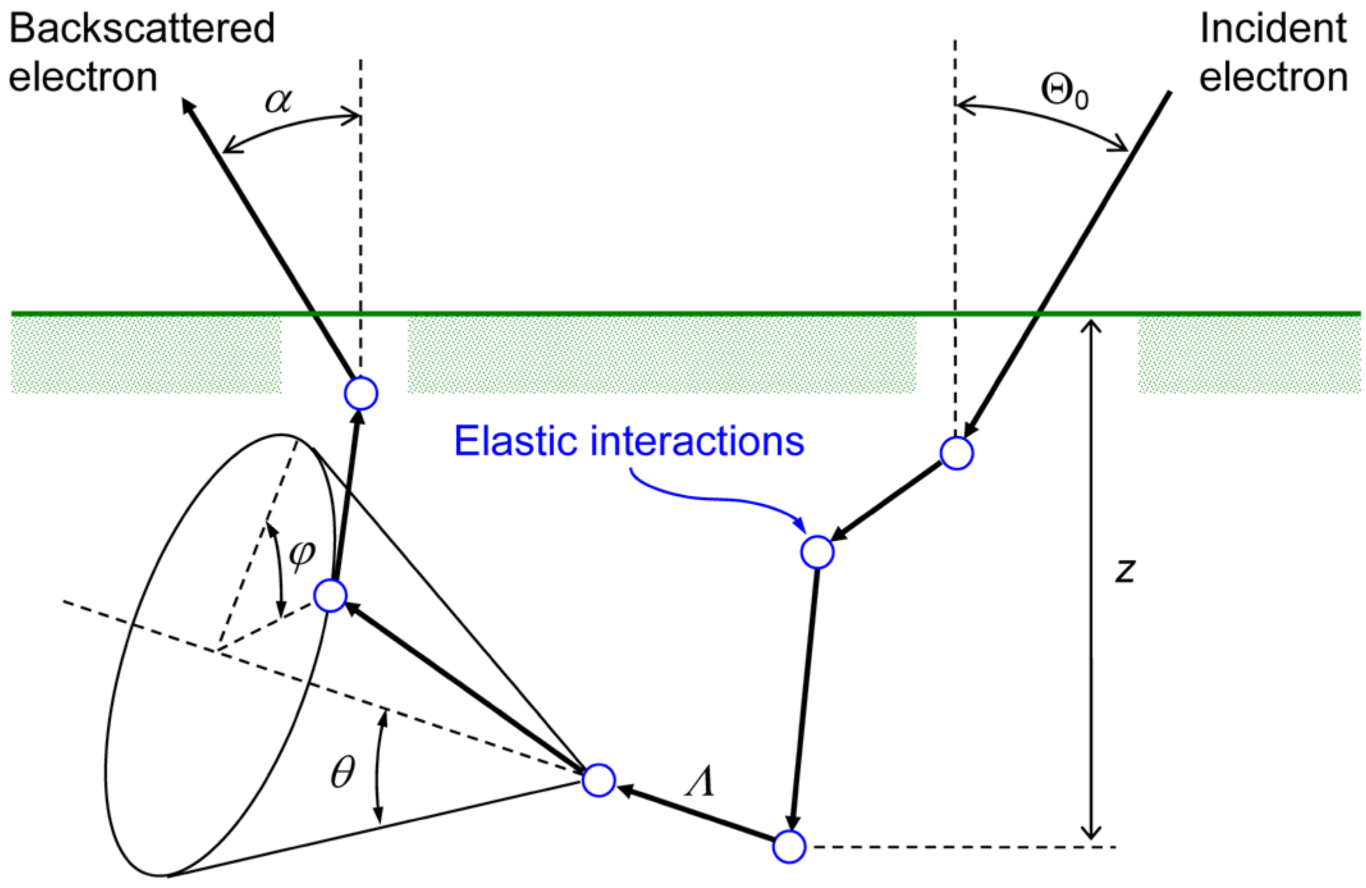

Fig. 2

http://rcin.org.pl

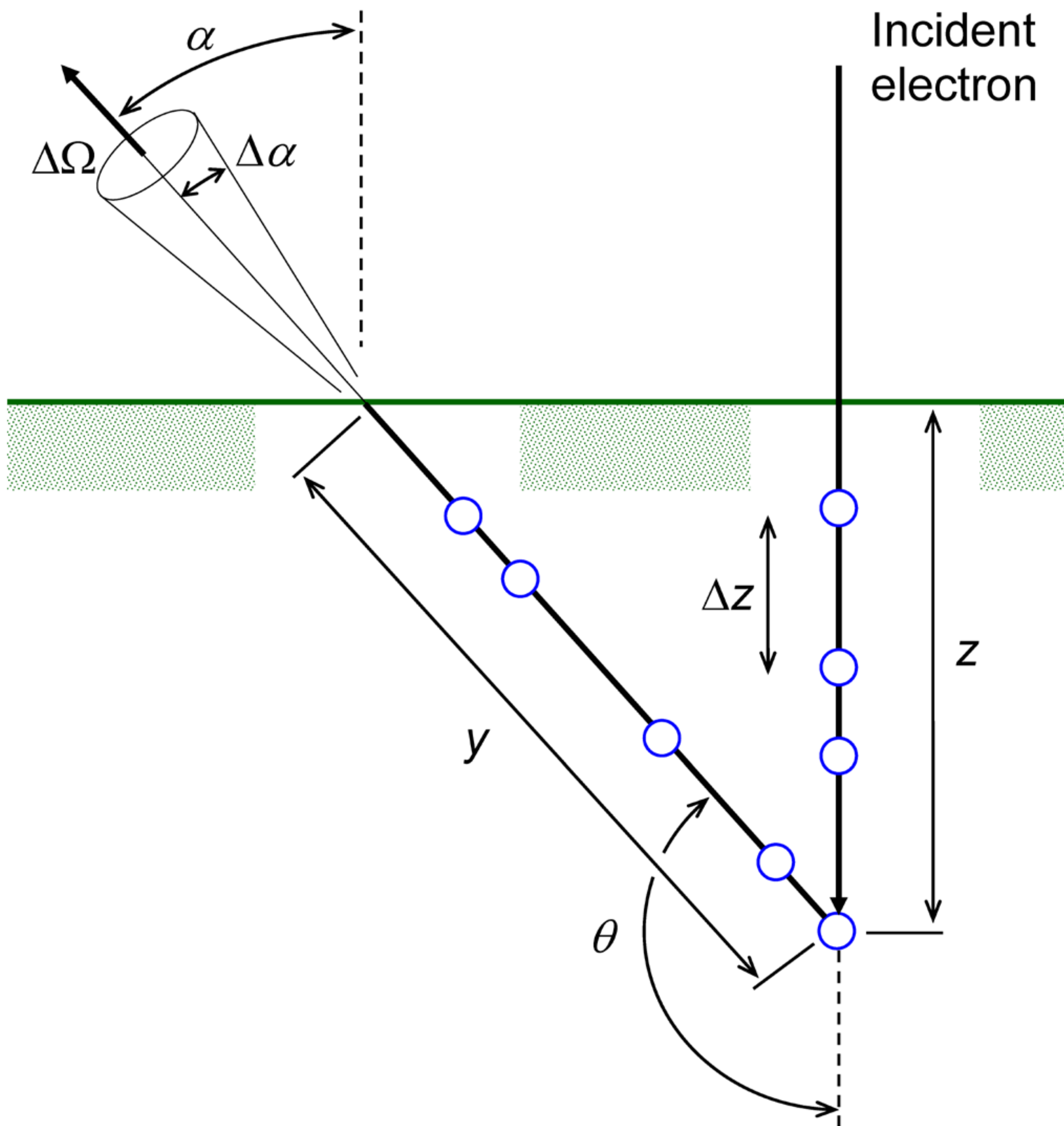

Fig. 3

http://rcin.org.pl

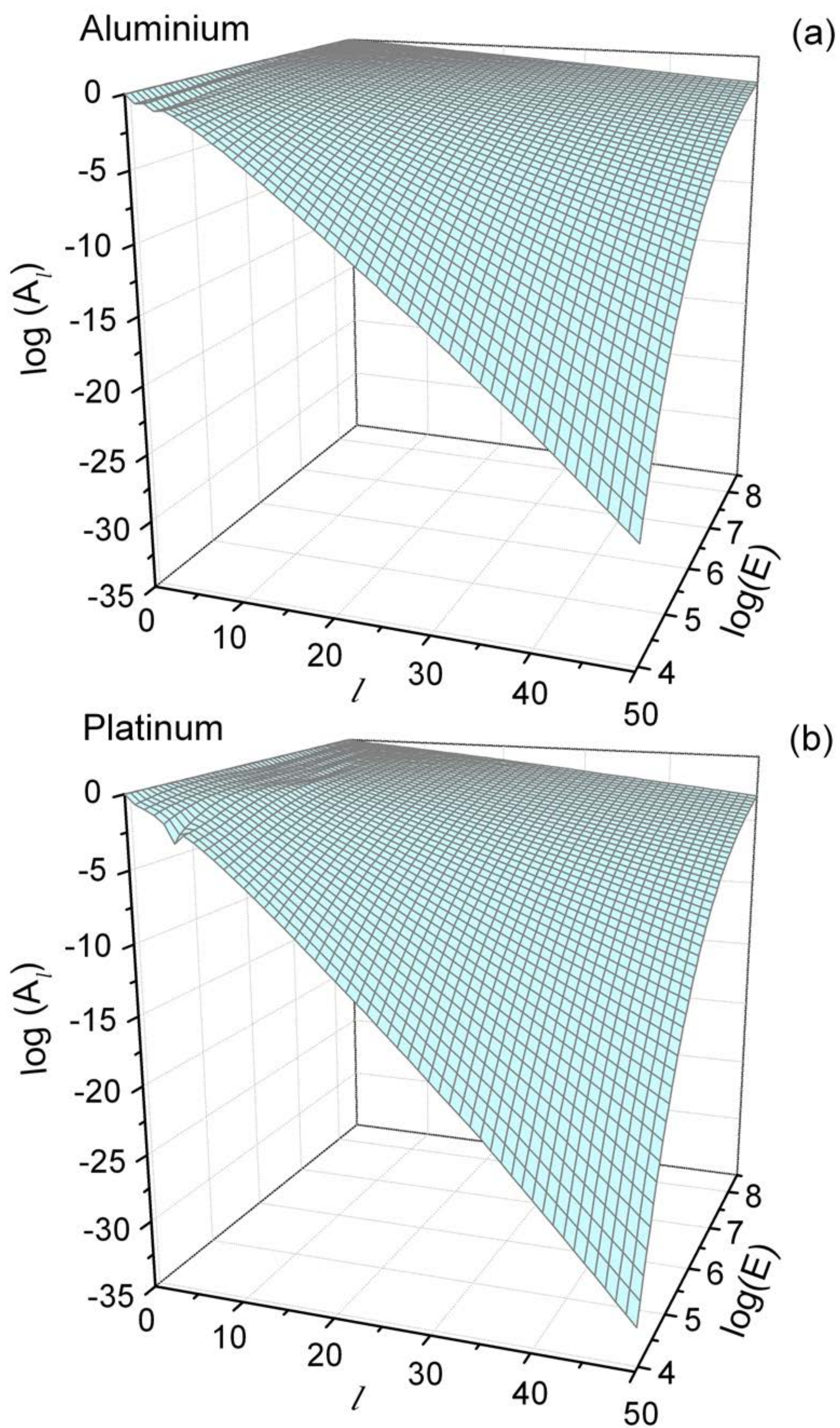

Fig. 4

http://rcin.org.pl

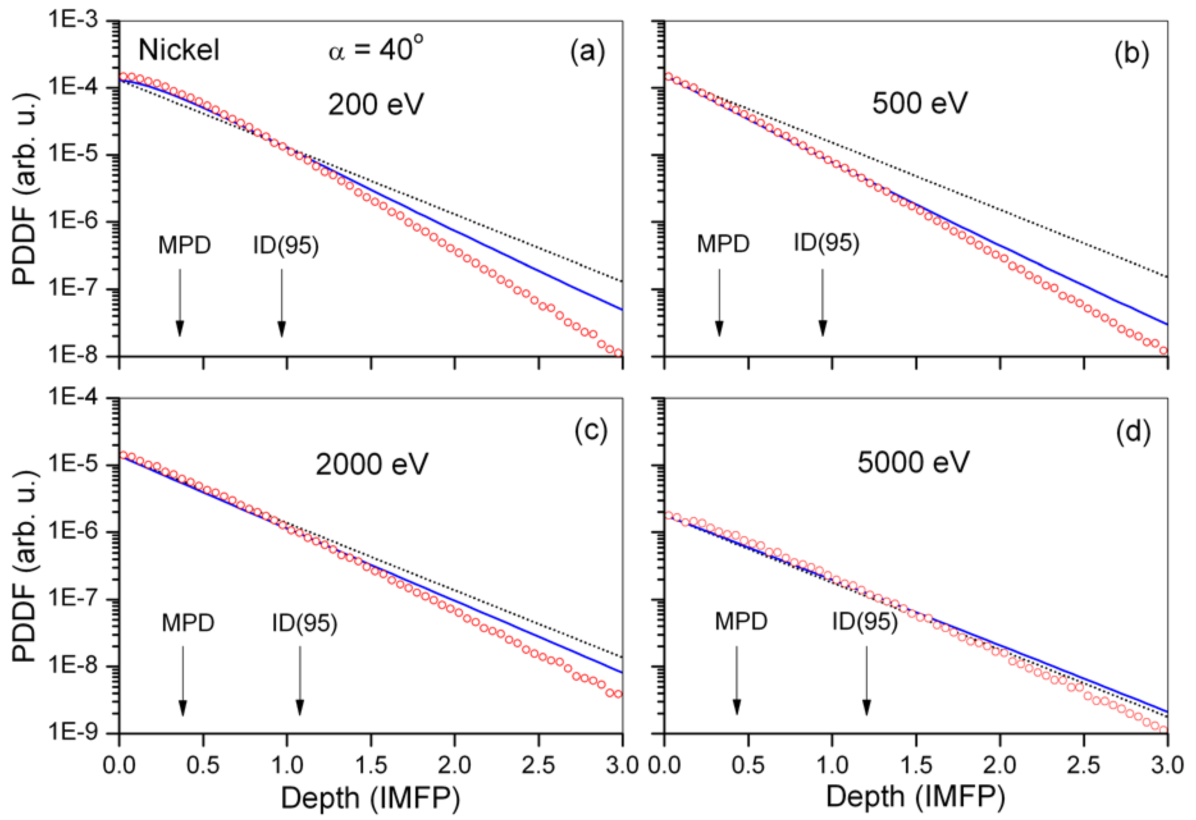

Fig. 5

http://rcin.org.pl

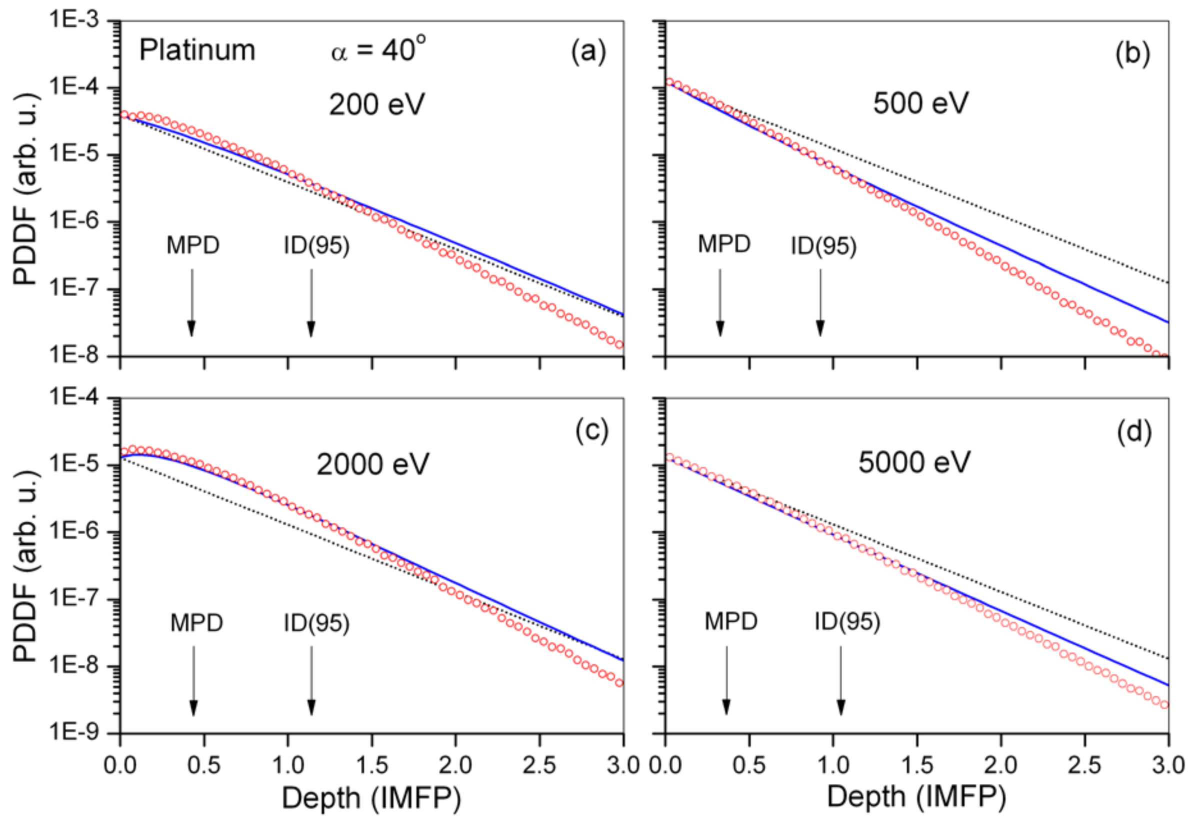

Fig. 6

http://rcin.org.pl

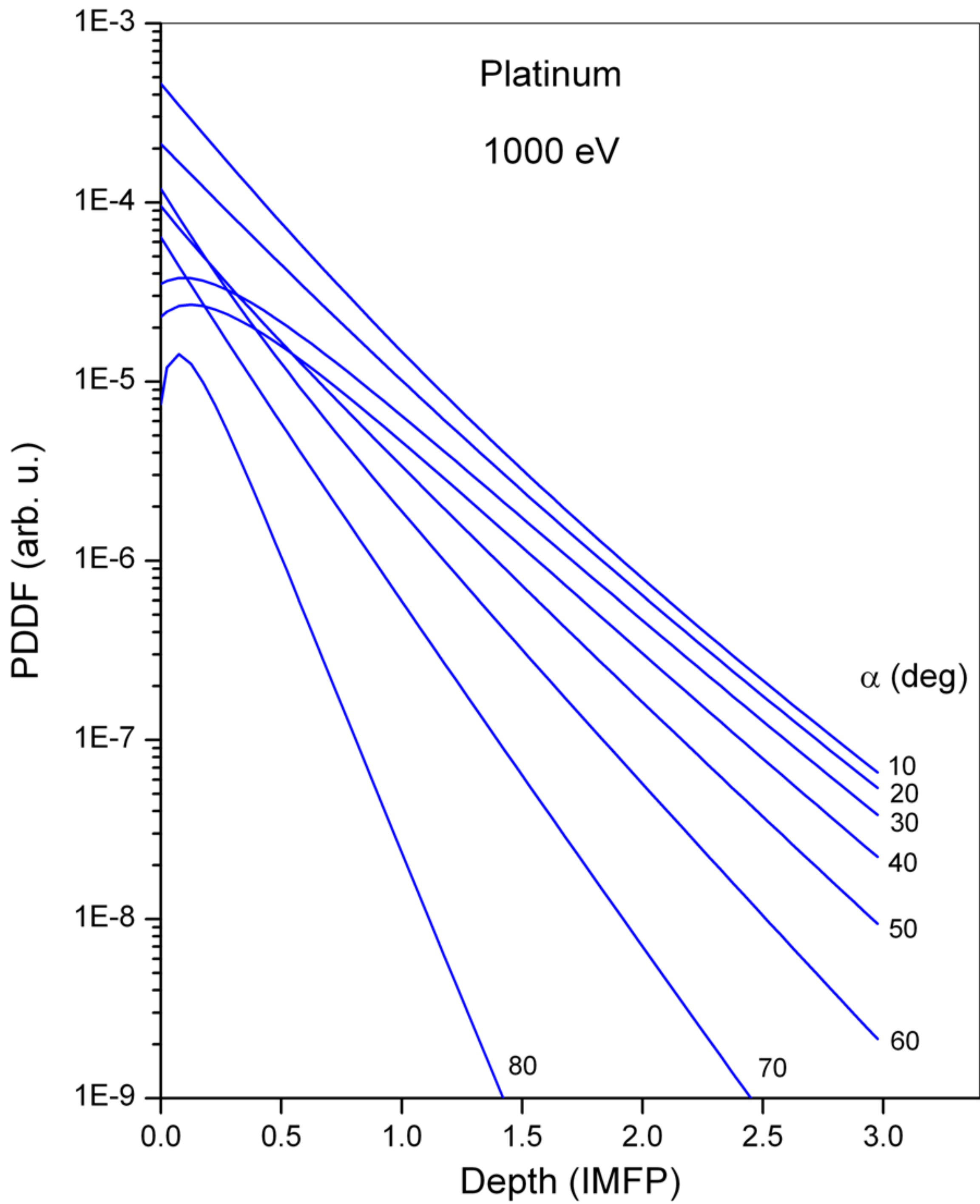

Fig. 7

http://rcin.org.pl

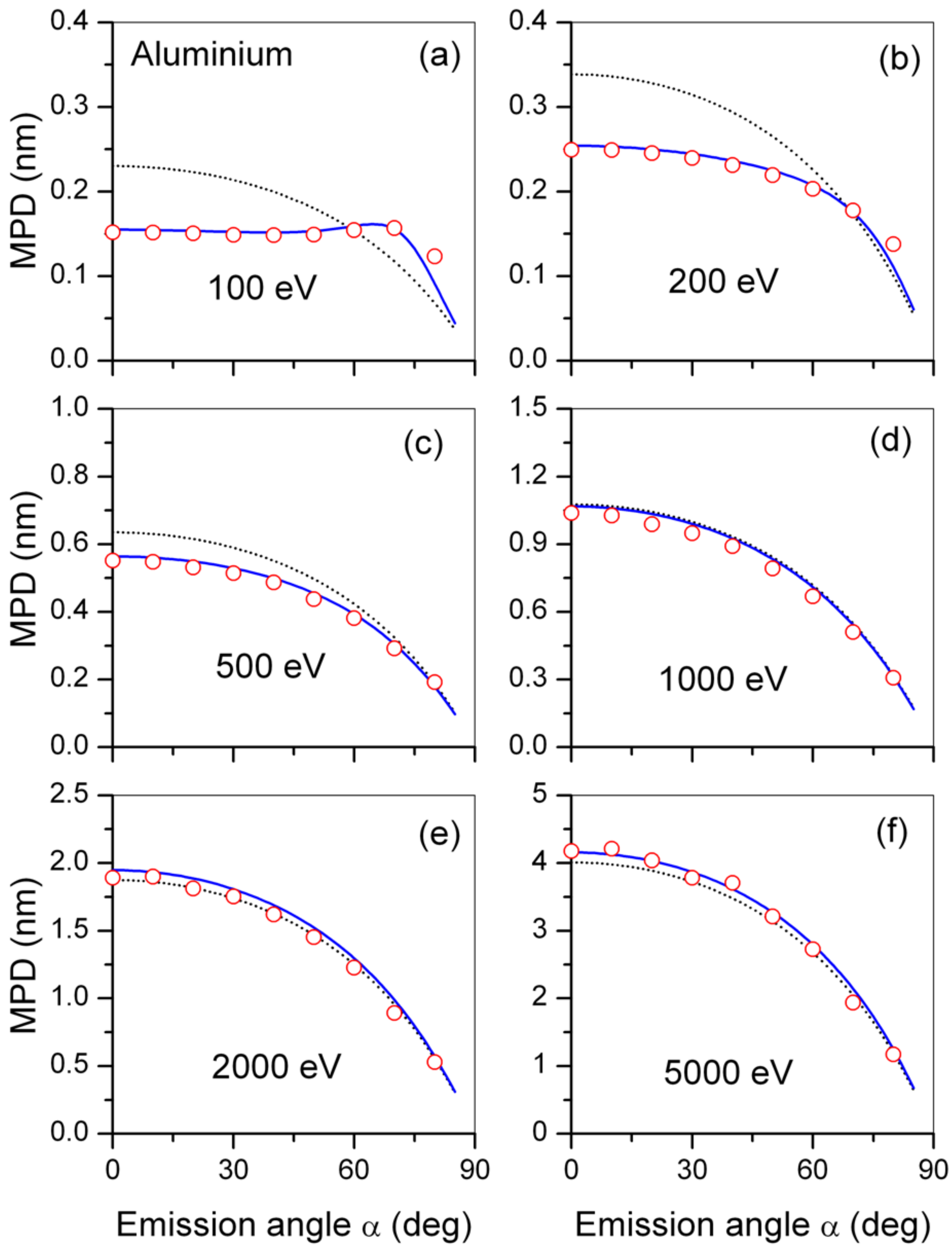

Fig. 8

http://rcin.org.pl

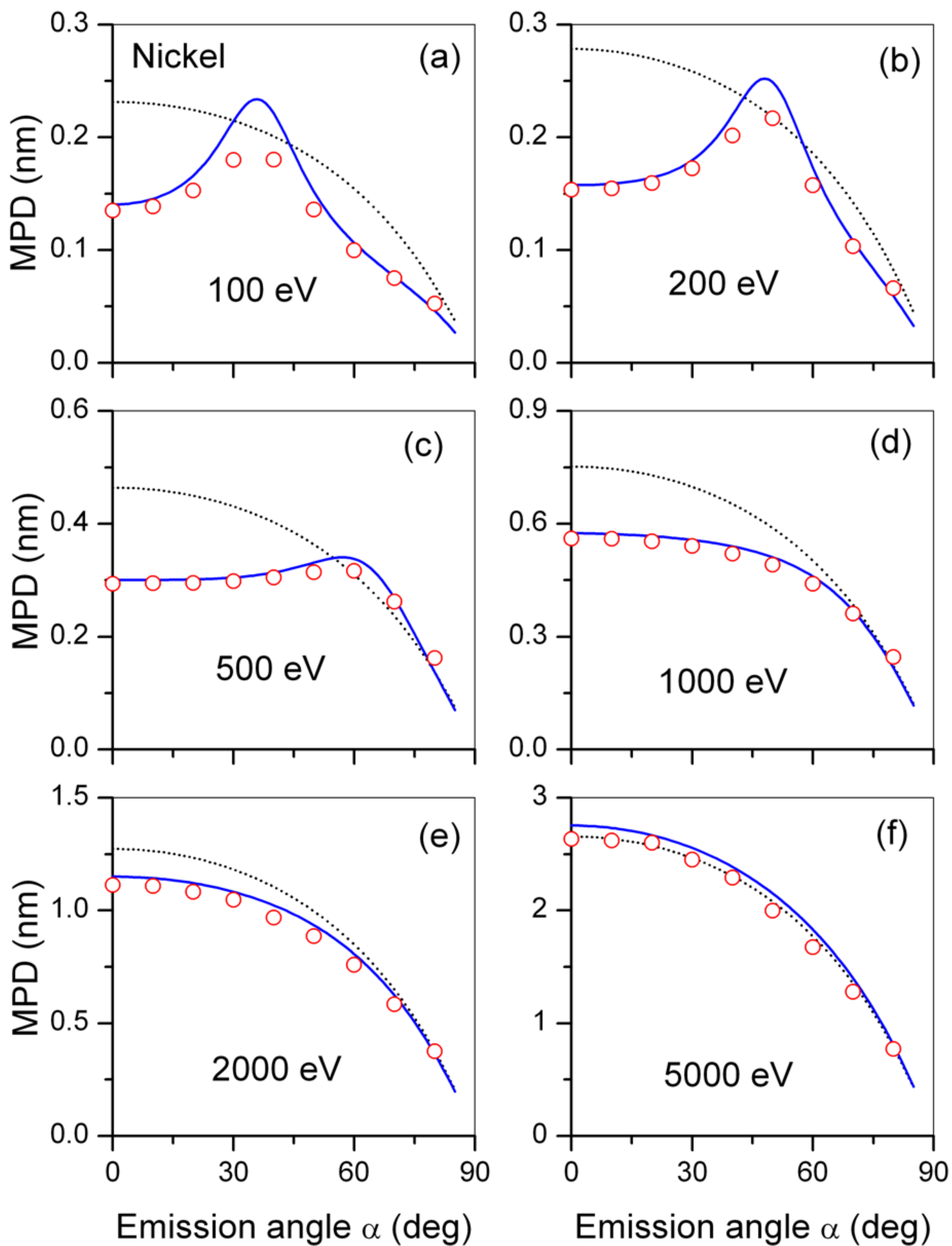

Fig. 9

http://rcin.org.pl

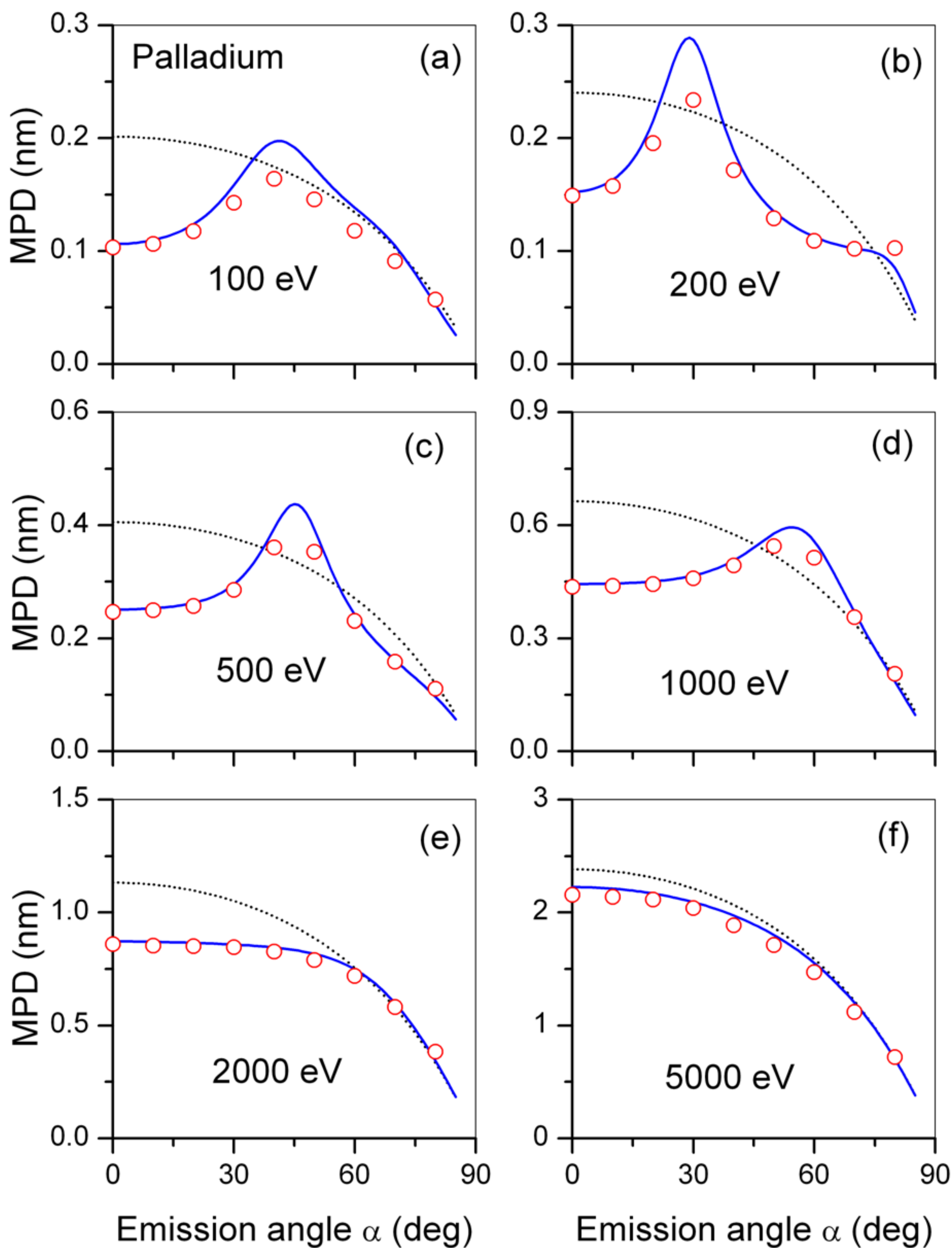

Fig. 10

http://rcin.org.pl

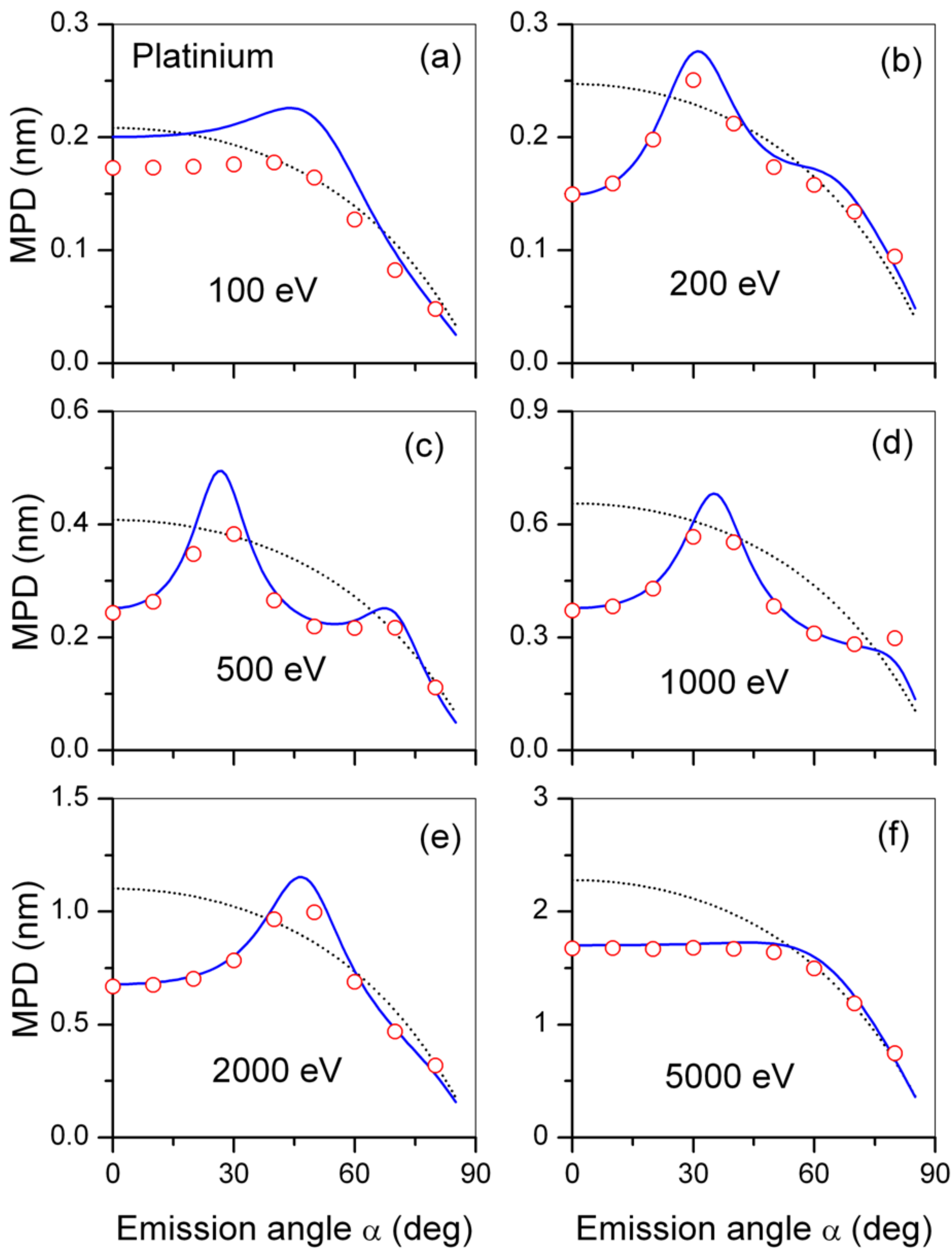

Fig. 11

http://rcin.org.pl

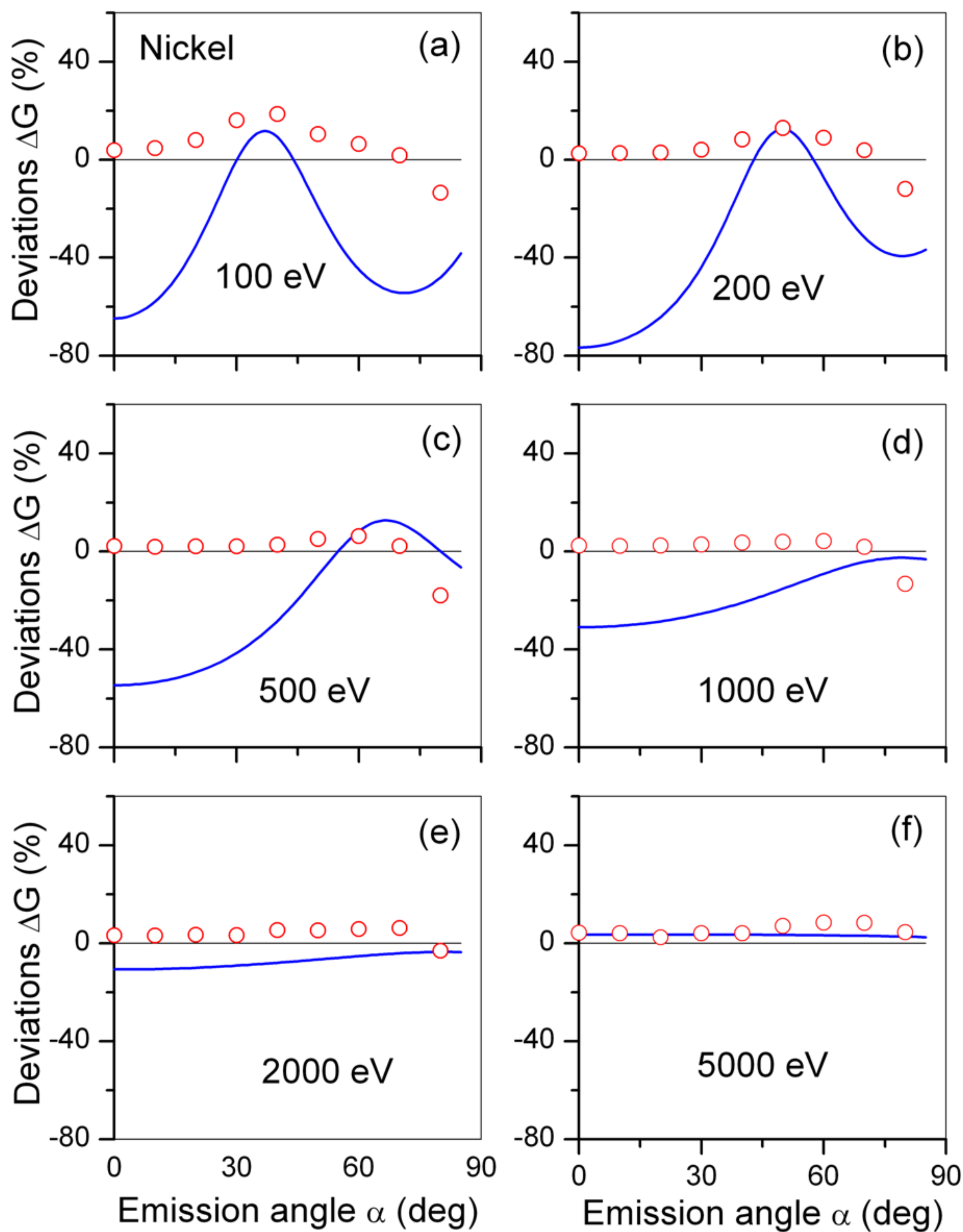

Fig. 12

http://rcin.org.pl

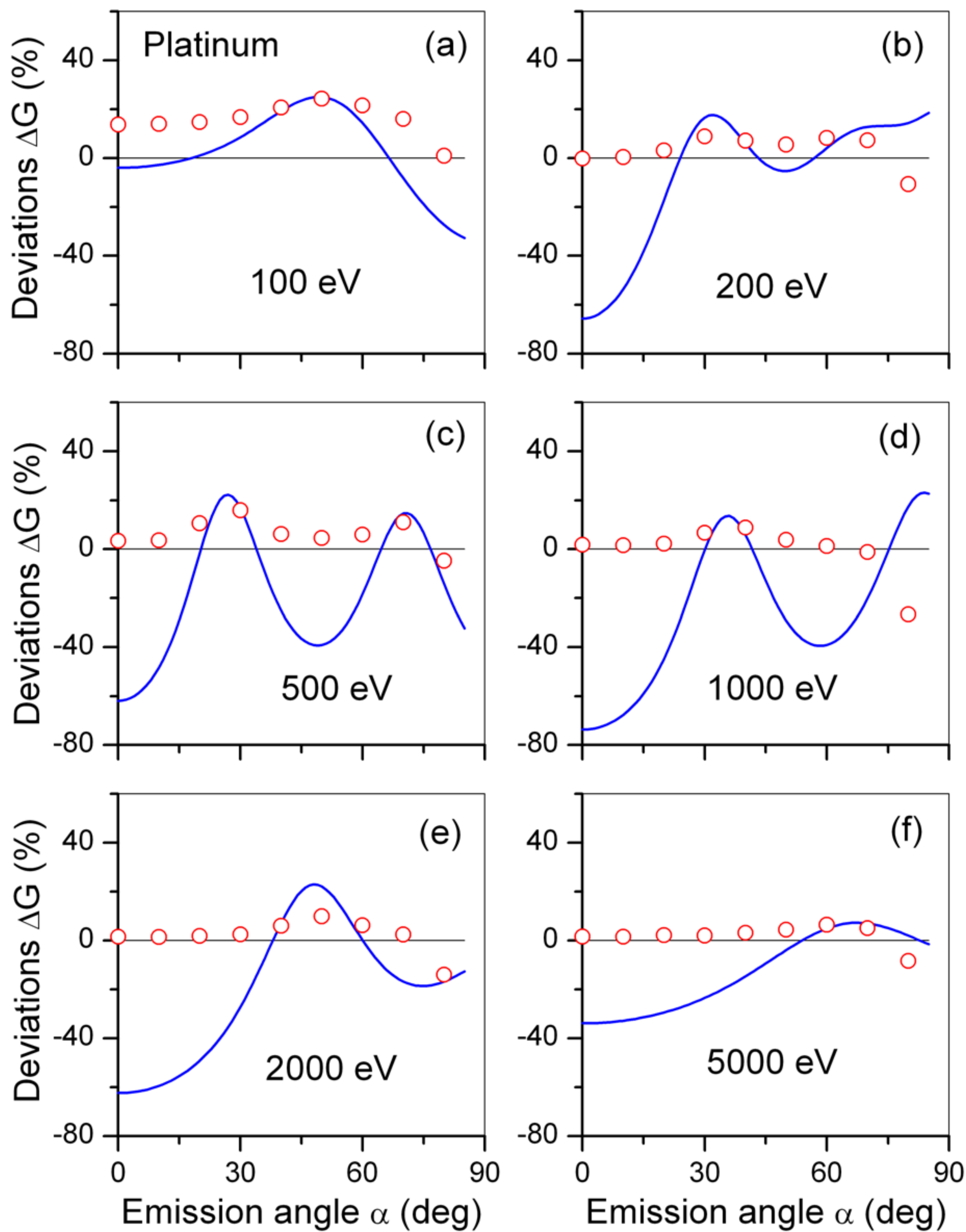

Fig. 13

http://rcin.org.pl

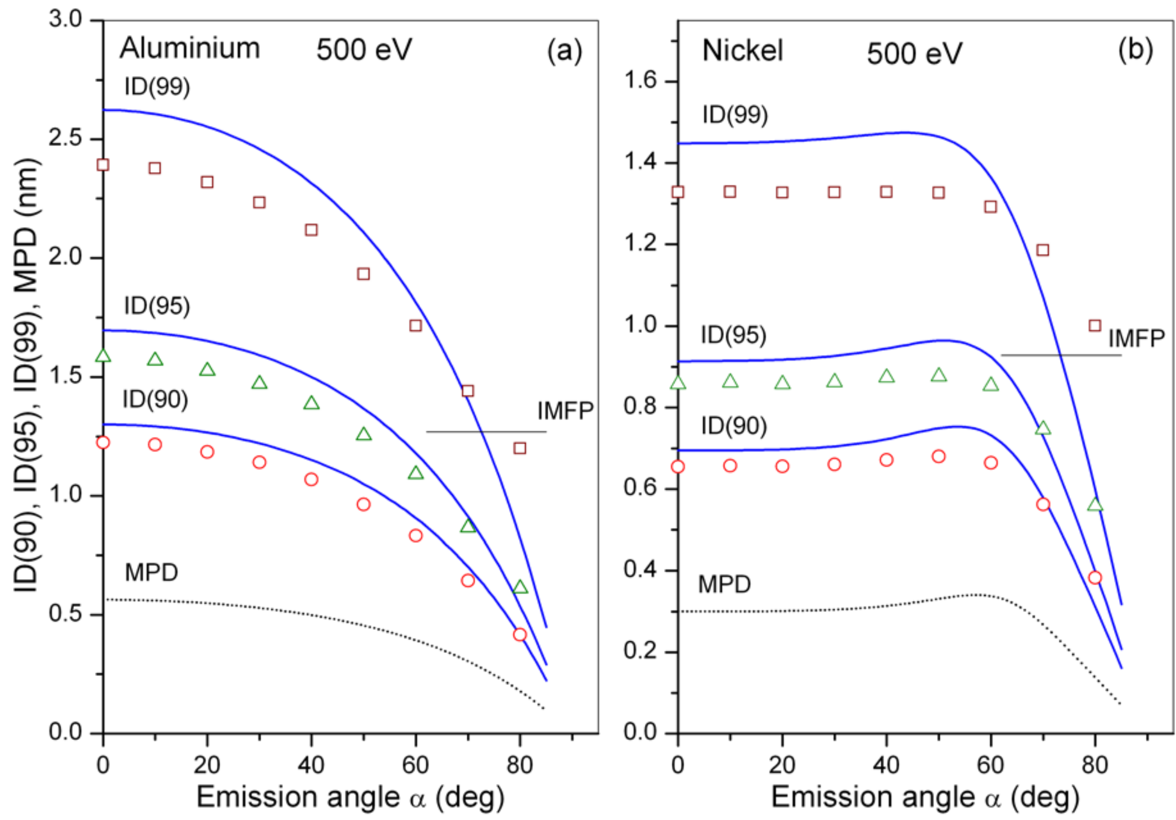

Fig. 14

http://rcin.org.pl

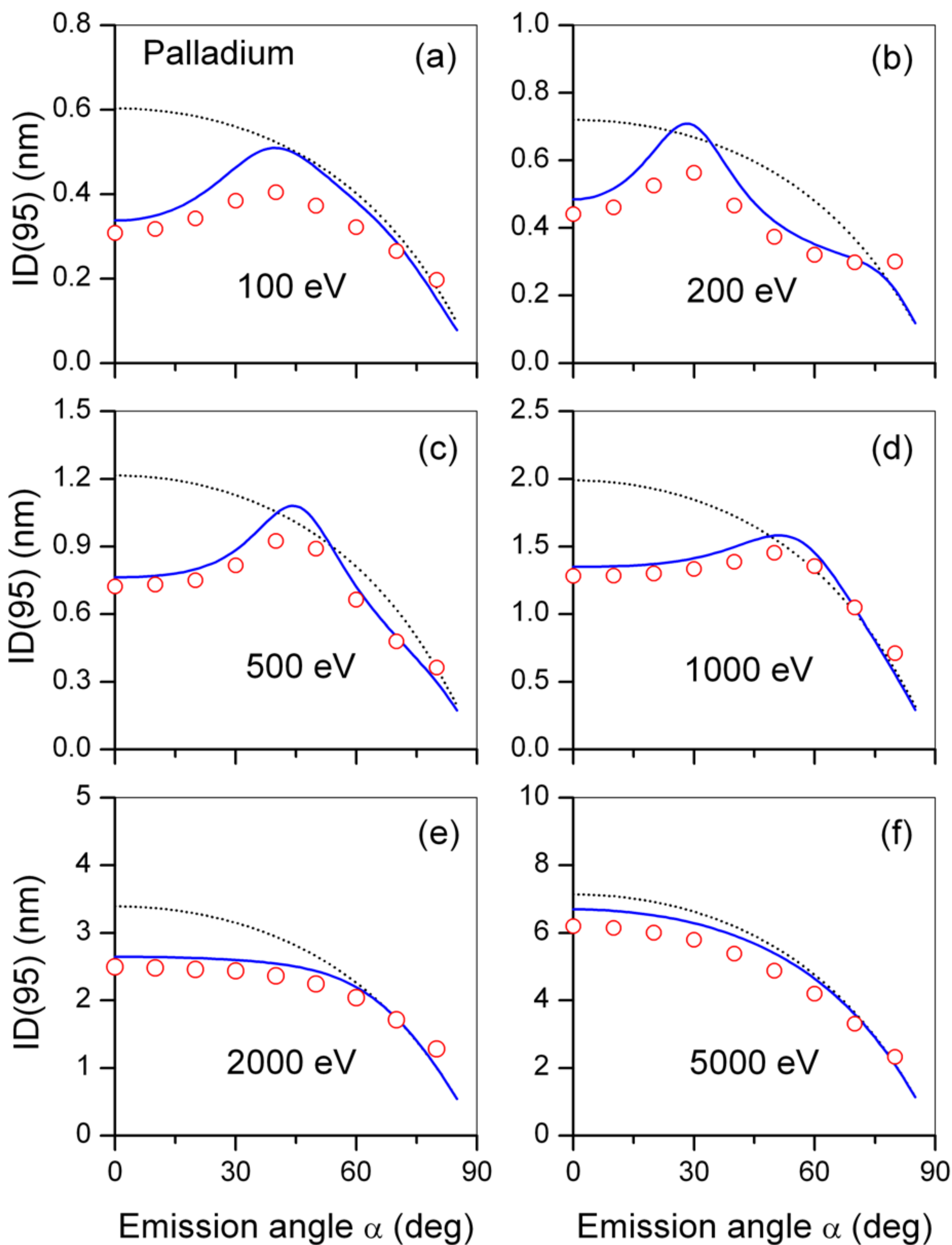

Fig. 15

http://rcin.org.pl

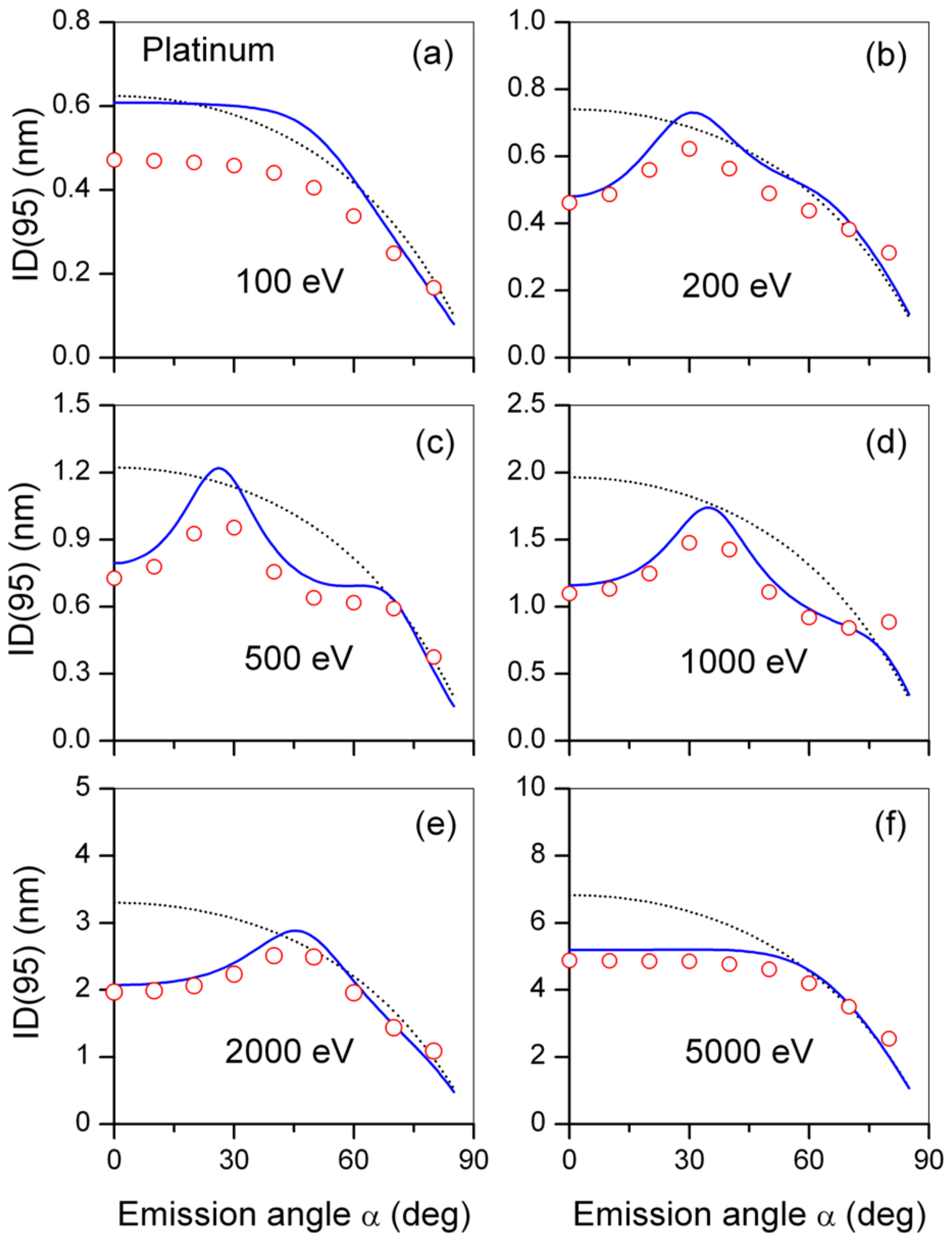

Fig. 16

http://rcin.org.pl

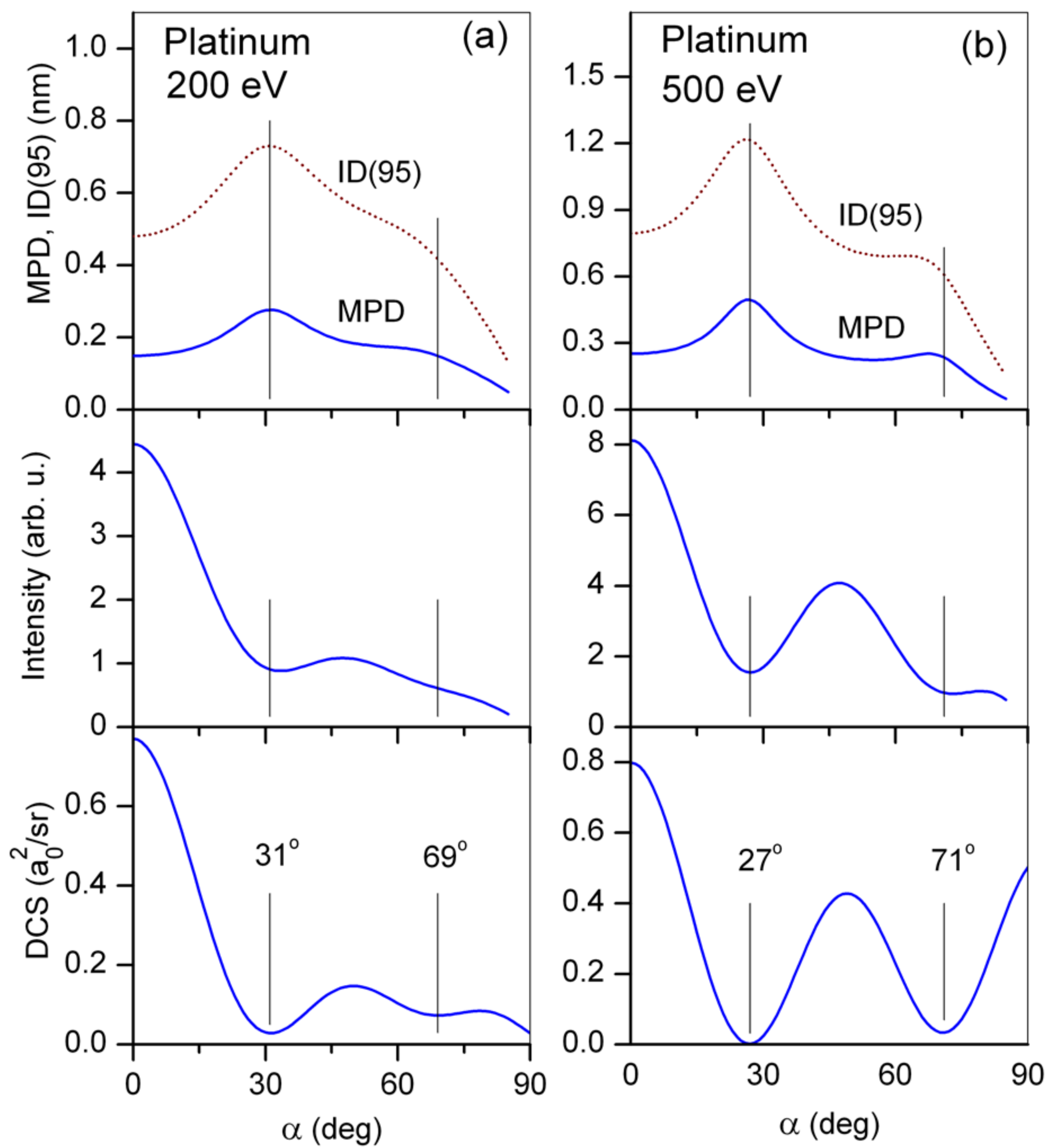

Fig. 17

http://rcin.org.pl

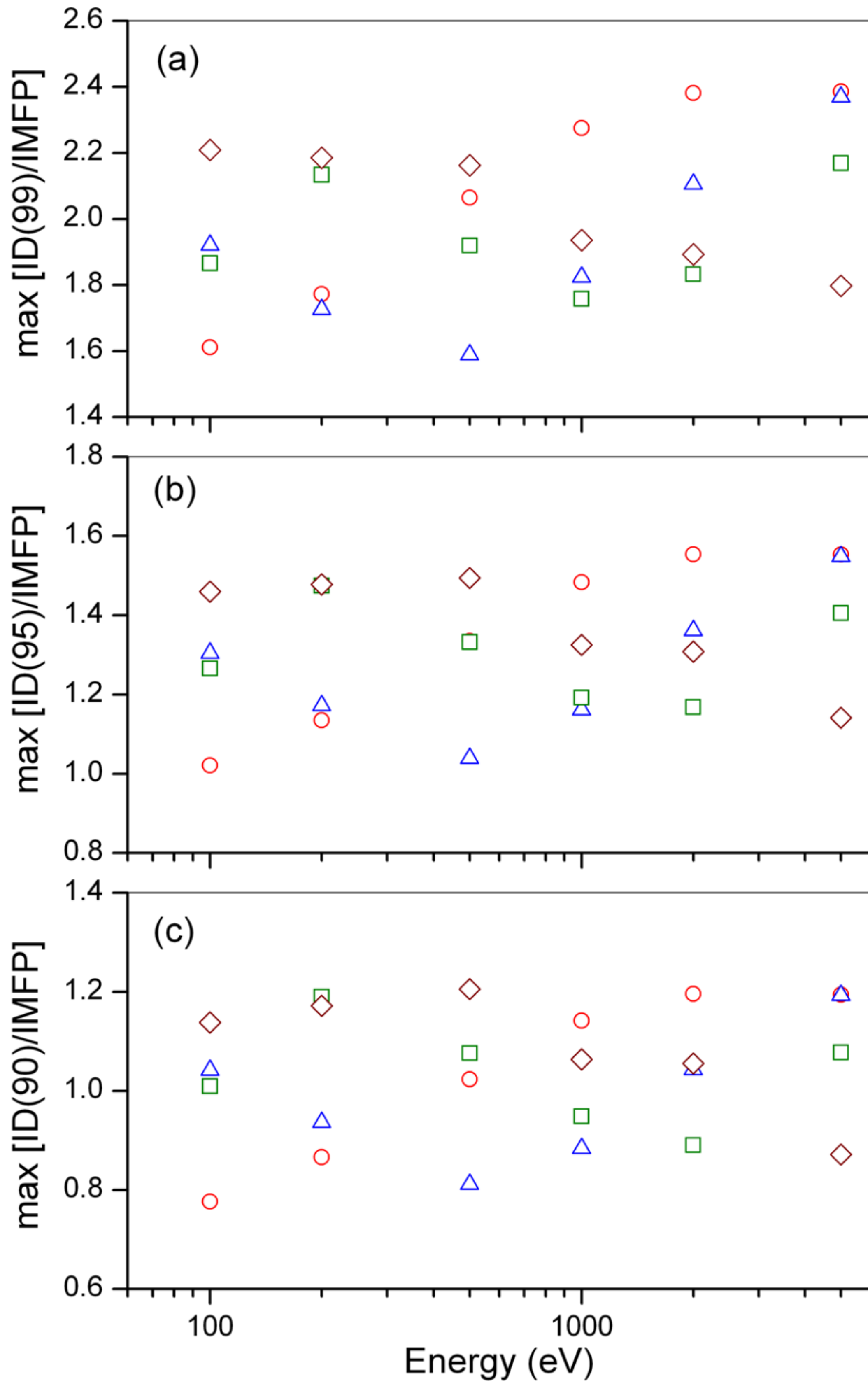

Fig. 18

http://rcin.org.pl

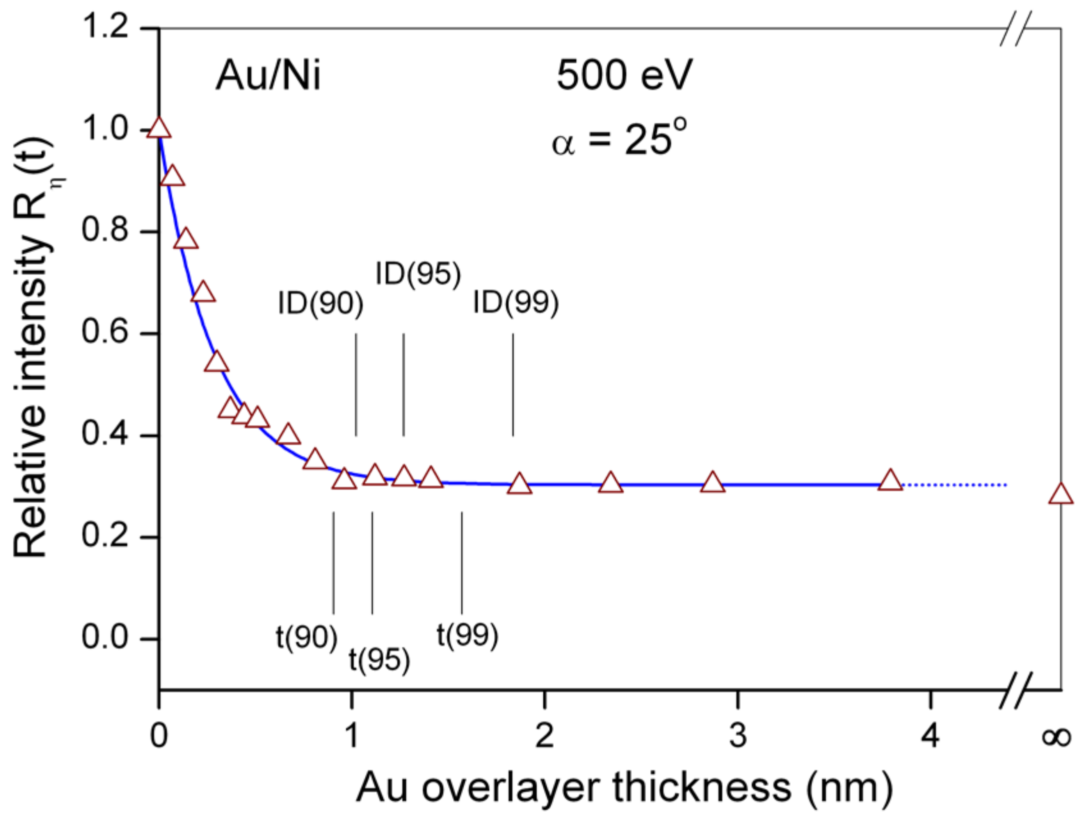

Fig. 19

http://rcin.org.pl